Characterization of a Middle Miocene Monogenetic Volcanic Field Buried in the Canterbury Basin, New Zealand – Part I

Alan Bischoff [a]*, Andy Nicol, Marcos Rossetti and Ben Kennedy

[a] *Department of Geological Sciences, University of Canterbury, Christchurch, New Zealand;*

alanbischoff@icloud.com *corresponding author

This is a non-peer reviewed preprint submitted to EarthArXiv.

It has been submitted on February 13, 2019 to Bulletin of Volcanology.

Characterization of a Middle Miocene Monogenetic Volcanic Field Buried in the Canterbury Basin, New Zealand – Part I

Buried volcanoes occur in great numbers within sedimentary basins around the globe. Over the last two decades, the knowledge of these 'fossil' volcanic systems has increased significantly due to improvements and availability of high-quality seismic reflection data. This series of two papers characterize a cluster of 31 middle Miocene volcanoes, currently buried by ca 1000 m in sedimentary strata of the Canterbury Basin, New Zealand. These volcanoes were imaged by high-quality 2D seismic lines and drilled by the petroleum exploration well Resolution-1, which recovered a monzogabbro intrusion and correlative volcanoclastic rocks. Here, we refer to this cluster of small-volume volcanoes as the Maahunui Volcanic Field (MVF). More than 40,000 km of high-quality 2D seismic lines correlated with data from six boreholes allows us to interpret the primary and secondary processes that form and modify these volcanoes now "fossilized" in the Canterbury Basin. Rock samples show high content of glassy shards, relics of bubble walls, spheroidal aggregates (armoured lapilli), fragments surrounding by a palagonite film, and broken phenocrysts, suggesting that MVF experiences submarine explosivity and subsequent flow transportation and deposition. XRF, SEM-EDS and petrographic analysis suggest a co-genetic correlation between both intrusive and volcanoclastic rocks. This correlation is reinforced by seismic reflection imagery of a saucer-shaped sill that likely fed volcanic eruptions onto the middle Miocene paleo-seafloor at the location of the Resolution-1 well. Miarolitic cavities and ophitic texture observed in the monzogabbro suggest that the saucer-shaped sill was injected at shallow depths, which is estimated to be around 950 m below the paleo-surface at the time of the intrusion. Integration of the results from petrographic and seismic reflection analysis allows us to interpret that the eruptions in MVF were entirely submarine (ca 500 to 1500 m), producing subaqueous equivalents of maar-diatreme and tuff cone volcanoes.

Keywords: buried volcanoes; monogenetic field; seismic reflection; submarine eruptions.

Introduction

Buried volcanoes are common in New Zealand and in sedimentary basins around the globe (e.g. Field et al., 1989; Holford et al., 2012; Planke et al., 2017; Barrier et al., 2017). Characterization of these "fossil" volcanic systems requires integration of large datasets of 2D and 3D seismic surveys with biostratigraphic, geochronological, geochemical, petrophysical and petrographic information from drilling wells (e.g. Planke et al., 1999; Single and Jerram, 2004; Schofield et al., 2016; McLean et al., 2017). The interpretation of these datasets is typically made by adopting a multidisciplinary approach that correlates insights from disciplines such as stratigraphy, structural geology, and volcanology into a unified model to explain the genesis and evolution of these buried volcanic systems (e.g. Herzer, 1995; Planke et al., 2000; Giba et al., 2013). Information from these complementary disciplines enables us to understand the spatio-temporal relationship between the volcanic and sedimentary elements within the buried volcanic systems (e.g. Huafeng et al., 2015; Bischoff et al., 2017; Infante-Paez and Marfurt, 2017). This background information is the basis to reconstruct the paleo-morphology of buried volcanoes and the paleo-environmental scenarios in which the volcanic events occurred within the host sedimentary basins (e.g. Magee et al., 2013; Reynolds et al., 2016; Bischoff, 2019).

In this series of two papers, we characterize a cluster of 31 middle Miocene volcanoes, currently buried by ca 1000 m of sedimentary strata in the offshore Canterbury Basin, eastern side of Zealandia (Figure 1). For the purposes of these papers, we refer to this cluster of buried volcanoes as the Maahunui Volcanic Field (MVF), which is the Māori name for the stretch of coast south of Banks Peninsula (aka Canterbury Bight) and immediately adjacent to the study area. In the part I of this study, we introduce the topic and the regional geological setting, explaining the methods for characterizing buried volcanoes from seismic and well data, and presenting the results

from small-scale detailed petrographic analysis, seismic and paleo-environmental interpretation of in the area of the well Resolution-1 (Figure 1). In part II, we up-scale interpretations to a regional scale, based on seismic stratigraphic mapping techniques, presenting the seismic morphological reconstruction of the volcanoes on the MVF, and the geological evolution of this volcanic field within the Canterbury Basin.

To conduct this study, we use high-quality 2D seismic lines, data from six petroleum exploration wells (Figure 1), and insights from dozens of outcropping, submerged, and buried volcanic systems imaged by 3D seismic surveys from New Zealand sedimentary basins and elsewhere. The compiled datasets are complementary, providing information about the rock-types, eruptive styles, magma-sediment interactions, volcanic morphologies, and volcanic architecture within the basin strata. Most data from analog volcanic systems were compiled from the literature, although we also have made our own observations and interpretations from onshore (e.g. Waiareka-Deborah Volcanic Field and Banks Peninsula Volcanic Complex) and offshore examples in the Canterbury (e.g. Waka-3D seismic survey) and Taranaki basins (e.g. Romney and Vulcan-3D seismic surveys). Insights from this work help to improve understanding of the architecture of volcanic systems within sedimentary basins, which can be applied on the exploration of commercial geoenergy resources such as hydrocarbons and geothermal energy in association with buried and active monogenetic volcanic systems elsewhere.

Geological Setting

Sedimentation in the Canterbury Basin began in the middle Cretaceous (ca 112-105 Ma) and was synchronous with rifting, prior to the separation of Zealandia from west Antarctica and Australia (e.g. Mortimer et al., 2004). Lithospheric extension created NE-SW and E-W grabens in the Canterbury Basin, predominately infilled by

non-marine late Cretaceous sediments (Strogen et al., 2017). Post-rift quiescence and thermal subsidence promoted the deposition of marine sediments during the Paleogene, culminating with maximum transgression during the late Oligocene (Field et al., 1989; Ballance, 1993). Since the early Miocene, the present oblique-convergent boundary between the Pacific and Australian tectonic plates has produced tectonic cycles of uplift and erosion of the western border of the basin, with rapid progradation of a thick sequence of continental and marine sediments into the Canterbury Basin (Suggate et al., 1978; Kamp et al., 1992; Batt et al., 2004; Lu et al, 2005; Figure 2; Figure 3).

Volcanism occurred semi-continuously during the geological evolution of Canterbury Basin (Figure 1). During the Cenozoic, the Canterbury Basin and south-eastern Zealandia experienced widespread and long-lived intraplate volcanism. These magmatic events are not adequately explained by mantle plume or extensive lithosphere thinning models (e.g. Morgan, 1971; Weaver and Smith, 1989 apud Timm et al., 2010). Two different models have been proposed to explain the atypical magmatism in the Canterbury region: sudden detachment and sinking of a remnant late Cretaceous subducted slab (Finn et al., 2005), and asthenosphere upwelling induced by removal of parts of the subcontinental lithosphere throughout the Cenozoic (Timm et al., 2010). Independent of the geodynamic processes that control this Cenozoic magmatism, the observed products are primarily mafic in composition, and formed both monogenetic volcanic fields such as the Waiareka/Deborah and Waipiata Volcanic Fields (e.g. Coombs et al., 1986; Németh and White, 2003), and large polygenetic volcanic complexes like those from Banks and Otago Peninsulas (e.g. Coombs et al., 1960; Sewell, 1988). In the offshore Canterbury Basin, several late Cretaceous to Pleistocene buried volcanoes and intrusive bodies have been mapped using seismic reflection data (Field et al., 1989; Blanke, 2010; Bischoff, 2016; Barrier et al., 2017; Figure 1).

However, little is known about the eruptive histories of these systems, which is mainly due to a lack of detailed studies and direct geological information (less than a dozen of wells have recovered these volcanic rocks).

The MVF are located ca 40 km south and offshore of Banks Peninsula. In the study are Miocene volcanic and intrusive rocks were first identified in the petroleum exploratory Resolution-1 well, which was drilled in 1975 about 75 km offshore Ashburton (Figure 1; Figure 3). This borehole penetrated volcanoclastic rocks interbedded with bathyal siltstones of Waiauan age (12.7 to 11 Ma) from 1103.5 to 1220 m, and intersected a coarse-grained intrusive body at 1911 m, which was K-Ar dated at 12 ± 2 Ma (Milne, 1975). Successive authors tentatively correlated these rocks with outcropping volcanic rocks of Banks Peninsula, Acheron Outlier intrusions (Milne, 1975), and Harper Hills volcanics (Field et al., 1989; Figure 1). Banks Peninsula is a large polygenetic composite-shield volcanic complex mainly erupted subaerially during the late Miocene (Sewell, 1988). Harper Hills Basalts comprise a sequence of subaerial tholeiitic lava flows K-Ar dated at 10.5 ± 0.3 Ma (Carlson et al., 1980; Browne, 1983), and associated volcanic muds (Coalgate Bentonites), basalt dikes (Bluff Basalt), and well bedded volcanoclastic rocks (Sandpit Tuff). Biostratigraphic dating suggests that the Sandpit Tuff dates either from Waiauan (12.7 to 11 Ma) or Tongaporutuan (11 to 7.2 Ma), according to Carlson et al., (1980) and Browne (1983). Acheron Outlier intrusions are tholeiitic gabbros forming a large irregular laccolith emplaced along Cretaceous to Paleocene paralic sedimentary rocks of the Eyre Group and were most likely intruded into these rocks during the Oligocene (Eady, 1995). Results from this work indicate that the MVF is an independent cluster of deep submarine monogenetic volcanoes. Further studies and new seismic data would be necessary to map the total area of MVF and a possible correlation with co-genetic outcrops inland.

Methods and Limitations

Many important aspects of the geology of the study area rely on consideration of biostratigraphic and lithological data from the Resolution-1 well. Because of this, the structure of this work is designed to initially provide the reader with small-scale petrographic and paleoenvironmental information at the location of the Resolution-1 well (part I) and to progressively up-scale interpretations to a regional scale, based on seismic stratigraphic mapping techniques (part II).

We described and photographed relevant intervals of the Resolution-1 well at the New Zealand Petroleum and Minerals core-store. One drill-core of an intrusive rock from a depth of 1962.25 m and 13 composite cutting samples of volcanoclastic rocks at 10 m intervals between 1100 to 1230 m depth were collected to perform macro-and-microscopic petrographic, X-ray fluorescence (XRF), SEM (Scanning Electron Microscope) and EDS (Energy Dispersive Spectroscopy) analysis. Petrographic characterization of these cutting samples may have limitations due to a number of factors including their small original grain size, potential break-up of material during drilling operations, composite sample intervals that likely blend material from diverse beds, and difficulty to separate drilling mud from altered *in situ* volcanic fragments. Due to the high degree of alteration of some cutting samples, conventional sample washing to separate drilling mud from sampled material was not applied because most of the soft rock material would have been lost during the sieving process. Therefore, to prepare the samples we proceed by dry-and-wet manual “grain-by-grain” separation of potential volcanic fragments from drilling mud. XRF and SEM-EDS were then performed on samples from selected intervals that contain igneous rocks. Qualitative XRF analysis was conducted using an Olympus Vanta handheld analyzer calibrated to perform a bulk geochemistry analysis of the total samples for one sample from 1962.25 m depth (intrusion) and three samples from 1130 to 1160 m depth (volcanoclastics).

SEM and EDS analysis were conducted at the Electron Microscopy Centre at the University of Canterbury to analyze the elemental geochemistry of fragments collected from a depth range of 1140 to 1150 m (volcanoclastics), and to produce microscopic images of the morphology of these fragments.

Ten regional chronostratigraphic surfaces for early Miocene to Modern Seabed were mapped in detail: Basement (pre-Cretaceous), top Mata (Cretaceous), top Thanetian (Paleocene), Top Arnold (ca Oligocene), top Pareora (ca 15.9 Ma), top Southland (ca 11 Ma), top Taranaki (ca 5.3 Ma), top Opoitian (ca 3.7 Ma) and modern seafloor (Figure 2). Prior to mapping, the seismic reflection lines from the New Zealand Petroleum and Minerals (NZPAM) Kingdom© project were checked and calibrated with check-shot surveys from the Resolution-1 and Clipper-1 wells (Milne, 1975 and Hawkes and Mound, 1984). The depths of chronostratigraphic markers and formation tops were verified and, where necessary, corrected using the revised biostratigraphy of Canterbury Basin published by Schiøler et al. (2011). Next, we mapped two important early Miocene (eM) and late Miocene (lM) unconformities, based on the observation of seismic features such as types of stratal terminations and depositional trends associated with that surface (e.g. Catuneanu, 2006), following criteria for "sequence boundary" *apud* Hunt and Tucker (1992). In addition, we proceed with a seismic volcano-stratigraphic analysis (e.g. Planke et al., 1999) for the study area by mapping the lateral continuity of the pre- and post-eruptive surfaces (PrErS, PoErS) of MVF. This mapping correlate the first and last occurrence of middle Miocene extrusive rocks in the Resolution-1 well with seismic anomalies that could represent buried volcanoes of same age (Figure 4). Mapping of post-eruptive surfaces such as the post-degradational surface (PoDgS) and the post-burial surface (PoBuS) is an innovation of the seismic volcano-stratigraphic method introduced in Bischoff et al. (2017) and Bischoff (2019). These

surfaces are based on evidence of important erosional events that degrade the MVF edifices after volcanism had ceased (PoDgS), and on evidence of disturbances to basin sedimentation due to the progressive burial of the edifices (PoBuS).

Detailed seismic morphologic characterization (e.g. Figure 5) was conducted for each seismic anomaly that could represent a middle Miocene volcano buried in the study area (occurring between the PrErS and PoErS surfaces), and for all anomalies that could represent intrusive bodies within strata of the Canterbury Basin. The morphologic characterization of MVF is presented in the part II of this work.

Results from Petrography, XRF and SEM-EDS Analysis

In this section, we present the characteristics of five main groups of rocks related to the MVF: (1) Intrusive rocks emplaced into (2) host paralic to neritic sedimentary rocks, (3) bathyal mudstones and carbonates, and (4) bathyal siltstones interbedded with (5) volcanoclastic rocks.

Intrusive rocks (1911.5 to 1963 m)

The Resolution-1 well penetrates 51.5 m of intrusive rocks from 1911.5 to 1963 m, approximately 5 m of which was cored from 1958 to 1963 m. Macro and microscopic description of a core sample collected from a depth of 1962.25 m indicated a leucocratic, medium-grained hypidiomorphic medium-grade altered rock (Figure 6 and Figure 7). Primary minerals in this sample are plagioclase (70%) and augite (20%), with subordinate orthoclase and olivine (<10%). Plagioclases are usually 0.5 to 2.5 mm elongated euhedral to subhedral crystals, probably from andesine to labradorite composition based on their extinction angle, and are commonly altered to smectite, illite, and zeolite. Augite occurs as subhedral prismatic crystals up to 6 mm in diameter, which forms an ophitic texture with plagioclase. These textures and compositions are

common in diabase rocks and suggest an intermediate magma cooling rate at shallow depths (Walker, 1957). Clinopyroxenes in some cases are replaced by amphibole and biotite. Chlorite alteration is pervasive in some parts of the rock or associated with opaque minerals, and may indicate magma hydration and high temperature (ca 250° C) hydrothermal alteration. Olivine can be partially or totally replaced by iddingsite, which suggests an alteration in the presence of water (Smith et al., 1987). Miarolitic cavities occur in several parts of the core and reinforce the interpretation of a hypabyssal rock injected at shallow depths, which indicates that MVF melts were enriched in volatiles (Peretyazhko, 2010). Accessory minerals include apatite, opaques (ilmenite?) and zircon. We classify this rock using the QAPF diagram as an olivine-monzogabbro. The petrographic description presented in Milne (1975) classified some parts of this intrusion as a quartz-monzogabbro (however we did not identify quartz in our samples), and as a teschenite, due to the presence of analcite. Analcite (or analcime) is a tectosilicate from the zeolite group and can form as a primary igneous mineral in under-saturated volcanic rocks associated with hydrated magmas (Pearce, 1993). We describe rare crystals of analcite associated with radial zeolite, which always fill residual space and cavities. This suggests that analcite more likely is a secondary product of hydrothermal alteration rather than a primary mineral from the magma. However, a complete microscopic and nanoscopic analysis of the well core is required to test this interpretation. Results from the handheld qualitative XRF analysis indicate a bulk composition of ca 50% of silica (SiO_2), ca 17% of Al_2O_3, and high content of Fe, Mg, K, Ca and Ti, which may suggest a calc-alkaline magmatic series. Geochemistry analysis was conducted only with the attempt to verify a possible correlation between the middle Miocene intrusive and extrusive rocks. Further drilling, sampling, and analyses would be required to characterize the complete geochemistry of MFV.

Paralic to neritic host sedimentary rocks (1911.5 to ca 1335 m)

The monzogabbro sampled from the Resolution-1 well intruded Cretaceous-Paleocene paralic to middle neritic sedimentary rocks of the Broken River and Conway formations. These sedimentary rocks are composed of granular pebble size conglomerates, fine-grained white quartz-sandstones, associated with dark grey pyritic siltstones, and thin layers of carbonaceous mudstones. Hydrothermal effects are observed in these rocks extending ca 34 m above the intrusion, based on the occurrence of siltstones cross-cut by carbonate veins and abundant zeolites (Milne, 1975). Palynomorphs and miospores show an increasing degree of thermal alteration towards the intrusion (Schiøler et al., 2011). Onshore, analog gabbroid outcrops from the Oligocene(?) Acheron Outlier intrusions show evidence of thermal effects extending several tens of meters from the igneous rocks (Eady, 1995). Intrusions emplaced in organic-rich sedimentary rocks have the potential to elevate the temperature near the igneous bodies sufficiently high to generate thermogenic gas (e.g. Aarnes et al., 2015). This heating process can generate methane (CH_4), and can release high amounts of CO_2 (e.g. Delmelle et al., 2015; Sversen et al., 2018), together with acids such as H_2S (e.g. Iacono-Marziano et al., 2013; Robertson et al., 2015; Arnorsson et al., 2015). The upper Paleocene-Eocene part of this rock association is characterized by mudstones and fine-grained sandstones (Charteris Bay Sandstone), interpreted to be deposited in transgressive shallow-marine environments, in association to passive tectonic subsidence in the basin (Field et al., 1989; Schiøler et al., 2011). This rock association is locally interbedded with thin layers of tuffaceous rocks that probably correspond to material erupted from scattered vents in the Canterbury Basin (Figure 1) or with localized peperitic material.

Bathyal mudstones and carbonates (ca 1335 to 1284.1 m)

Bathyal mudstones and carbonates deposited from the Oligocene to early Miocene comprise light grey to brown mudstones (Ashley Mudstone) and light grey massive carbonate rocks (Amuri Limestone and Omihi formations). These units are typically poorly indurated and show gradual variation from silty mudstones to calcareous mudstones and wackestones (Milne, 1975; Figure 8). This rock association represents a period of maximum inundation of Zealandia, and in the study area, corresponds to the development of a condensed section attributed to a very low supply of terrigenous materials (e.g. Field et al., 1989). The contact between the Amuri and Omihi formation is unconformable with a time break of ca 13.5 million years, from the early Oligocene to early Miocene (unconformity O-eM; Figure 3; Figure 8). The origin of the O-eM unconformity is controversial and successive authors have interpreted it as the product of glacio- or tectonic-eustatic changes, sediment starvation during a high stand period, volcanism, or action of sea-bottom currents (e.g. Lever, 2007). Seismic reflection analysis shows that some funnel-like anomalies interpreted to represent maar-diatreme volcanoes have excavated into the upper part of these sedimentary rocks, which is the topic of the second part of this work. Rare tuffaceous material is locally described interbedded within this rock association, which likely was erupted from scattered vents in the Canterbury Basin (Figure 1).

Bathyal siltstones (1284.1 to 686.1 m)

From 1284.1 to 686.1 m, the dominant rock in Resolution-1 is a soft light grey siltstone (Tokama Siltstone) with sparse bioclasts and benthonic foraminifers (Figure 9A), deposited in a bathyal setting from the early Miocene to early Pliocene (Milne, 1975; Schiøler et al., 2011). These rocks are locally interbedded and blended with volcanoclastic material of the MVF (Figure 9B), which we characterized separately in

the section “Volcanoclastic Rocks”. During the formation of Tokama Siltstone (early Miocene to early Pliocene), three main biostratigraphic unconformities have been identified in the Resolution-1, each representing hiatuses of 1 to 3 Ma (Schiøler et al., 2011). These unconformities are interpreted to be formed by different tectonic pulses during the onset of basin inversion and compressional tectonics to NW of the study area, which is related to southward propagation of the Neogene Hikurangi subduction zone (Field et al., 1989; Kamp et al., 1992; Lu et al, 2005; Schiøler et al., 2011). Here, we refer to these unconformities as eM (early Miocene), lM (late Miocene), and eP (early Pliocene), according to their ages of formation (Figure 3).

To characterize in detail the paleoenvironment in which MVF has erupted, we subdivide the Tokama Siltstone into four depositional units, according to major paleo-bathymetric shifts identified in the biostratigraphic data (Schiøler et al., 2011) of the Resolution-1. These shifts are strictly related to the position of unconformities and are distributed in the well as follows: lower Tokama (1284.1 to 1260), middle Tokama (1260 to 1070), upper Tokama (1070 to 1016), and uppermost Tokama (1016 to 686.1). Table 1 and Figure 8 shows the main stratigraphic and paleo-environment characteristics of these units.

The lower Tokama was deposited during the late early Miocene, in a deep lower bathyal setting, with water depths ranging from 2000 to 1500 m (Figure 8). Its upper boundary is marked by a sharp transition to a lower bathyal setting (1500 to 1000 m), which is represented by the unconformity eM and its correspondent ca 1.5 Ma hiatus in the study area (Figure 8). The middle Tokama (which is interbedded with volcanoclastic rocks of the MVF) was deposited during the middle Miocene, in a relatively steady lower bathyal setting (1500 to 1000 m deep). This is evident by the biomarker species Sigmoilopsis schlumbergeri and Eggerella bradyi, often associated with Cibicides

robertsonianu, although the decrease in planktic towards the top of the middle Miocene interval points to an overall up-hole decrease in water depths (Schiøler et al., 2011; Figure 8). We place the onset of this base-level fall at ca 11 Ma, based on seismic stratigraphic analysis that shows an NW-SE progradation of clinoforms in a downlap relationship onto sub-horizontal reflectors into the basin, which indicates decreasing water depths in the area of Resolution-1 (Figure 4).

The onset of decreasing water depths marks the base of the upper Tokama, which is interpreted to represent a progressive shift from a lower bathyal to a middle bathyal setting (800-600 m), due to increasing sedimentary supply from the NW. During this period, all volcanic activity in MVF was extinct. The top of upper Tokama is marked by a sharp transition to an uppermost bathyal setting (400-200 m) and associated hiatus of ca 1 Ma in the study area (unconformity lM), which is the most important post-eruptive erosional event that impacts the morphology of the volcanoes in the MVF (PoDgS). The uppermost Tokama (Figure 8) was deposited during the late Miocene to early Pliocene in an uppermost bathyal setting. Seismic stratigraphic interpretation suggests a progressively shallowing in water depths up-sequence. The top of this depositional unit is evident by the occurrence of bioclastic mudstones, coquinas and sandstones of the Kowai Formation starting at 686.1 m, which marks the establishment of an outer neritic setting (100 to 200 m) in the area of Resolution-1, which occurred around 5.3 Ma (unconformity lM, Figure 3).

Volcanoclastic rocks (1220 to 1103.5 m)

The Resolution-1 well penetrates a 116.5 m thick sequence containing fragments of volcanoclastic rocks interbedded with siltstones of the middle Tokama depositional unit (Figure 8; Figure 9; Figure 10; Figure 11; Figure 12; Figure 13; Figure 14; Figure 15; Table 1). Macro and microscopic description of cuttings sampled from this interval

indicate poorly sorted (< 0.1 to 5 mm), hyalocrystalline, highly altered, non-welded fragments of leucocratic rocks, glass fragments and disaggregated crystals. Grain-size distribution is variable, usually comprising fragments with microcrystalline, microporphyritic and vitrophyric texture, and less common vitriclastic textures (Figure 11). Primary components include crystals of plagioclase and pyroxene, shards of glass (Figure 12; Figure 13; Figure 14), and common spheroidal aggregates (armoured lapilli?; Figure 15). Sandstone and limestone lithics (probably from Amuri and Omihi limestones, and Charteris Bay sandstone) are relatively abundant (Figure 15). Pervasive palagonite alteration is dominant, which is typically associated as devitrification of sideromelane glass (e.g. Stroncik and Schmincke, 2002), although some fresh fragments of glass and other minerals also occur (Figure 12; Figure 13).

Plagioclase usually are <0.1 to 1.5 mm elongated euhedral crystals, typically associated with microporphyritic and vitrophyric texture (Figure 11A and C). Often, plagioclase occurs as euhedral to anhedral broken phenocrysts in sharp contacts with the groundmass (Figure 11B and D), which could represent fragments of holocrystalline material crystallized in the magma chamber that was disaggregated during explosive eruptions (Best and Christiansen, 1997). Less commonly, some phenocrysts show rounded margins (Figure 11D), which may be a consequence of abrasion due to particle collision during magmatic transport, or mixing and recycling of material associated with multiple explosions into the deep crater zones of maar-diatremes volcanoes (e.g. White and Ross, 2011; Graettinger et al., 2016). Some rare phenocrysts show sieve texture and devitrified glass inclusions (Figure 11C), which could indicate disequilibrium phases in the magma chamber, high volatile content of the original melts, or rapid magma decompression (Nelson and Montana, 1992).

Glassy shards are very common in the samples of this interval and occur in a wide range of shapes and textures. Most commonly, shards are non-welded and present blocky and cuneiform shapes, and less frequently, cuspate, platy, splintery, and relics of bubble walls. Spall shards form friable fragments usually with cuneiform, blocky, splintery, and minor relics of bubble-walls (Figure 12). These fragments commonly show jigsaw-fit texture and occur in association with blocky fragments that contain microporphyritic cores (Figure 12). These textures are typically interpreted to indicate quenching and breakup of larger and less altered hyaloclastite fragments formed by thermal shock during rapid cooling (McPhie et al., 1993). However, these textures could also represent resedimented fragments of spatter clasts initially deposited around the margins of submarine vents during a process equivalent of fire fountains, which formed by an expanding flare of magma above the vent, and quenching of erupted due to its interaction with the ambient water (e.g. Cas and Giordano, 2014). Shards with cuspate, platy, splintery shapes and relics of bubble walls sometimes occur associated with poorly sorted and vesiculated rocks (Figure 13), which could be indicative of submarine strombolian eruptions (e.g. Deardorff et al., 2011; Cas and Giordano, 2014), although examples of these features are also observed in hyaloclastites and deposits of eruption-fed density currents (e.g. McPhie et al., 1993; White, 2000). Blocky, cuspate and platy shards also occur in association with fragments that contain very fine broken crystals, low vesicularity, pervasive alteration to palagonite, and lithics (Figure 14) which could indicate (but not define) phreatomagmatic fragmentation processes (e.g. Walker and Croasdale, 1971; MacPhie et al., 1993).

Often, fragments in this interval display spheroidal texture in two distinctive styles: i) very friable spherules that easily disintegrate when in contact with water, with an inner core (lithic?) and external aggregate of very fine particles circled by a

palagonite film (Figure 15); and ii) spherules moderately-to-well indurated and associated with pseudo-perlitic cracks, showing a devitrified (palagonite) inner core, a single concentric outer rim, and an external array of acicular crystals in a radial pattern (Figure 16). In both cases, the spherules are associated with a pervasive alteration to palagonite. The forms and texture of these spherules resembles both armoured lapilli that could be the product of eruption-fed density currents (e.g. White, 2000; Agirrezabala et al., 2017), and/or spherulites, which are commonly interpreted to indicate high-temperature devitrification of coherent volcanic glass and/or the presence of aqueous solutions in the magma (e.g. Marshall, 1961; Lofgren, 1970; apud MacPhie et al., 1993).

Given the uncertainties and limitations presented in the section Methods, it was not possible to confidently interpret these rocks as primary eruptive or resedimented volcanoclastics. Some petrographic features (poorly sorted and polymictic material blended with Tokama Siltstone, and presence of rounded clasts) point in the direction of resedimented volcanoclastics. However, material blending could be caused by drilling issues, or could represent the distal products of submarine pyroclastic plumes that incorporated lithoclasts during magma fragmentation and transport (e.g. White, 2000). In contrast, wireline-logs of Resolution-1 show sharp log-facies contacts at the boundaries between volcanoclastics and siltstones (Figure 8), which commonly represent abrupt composition changes in lithofacies and could point towards a primary volcanoclastic source. In addition, seismic facies show constant lateral thickness in the volcanoclastic interval (Figure 17) and are not confined to valleys, which is characteristic of subaerial pyroclastic surges (e.g. Cas and Wright, 1992), and may indicate similar process as observed in eruption-fed density currents (e.g. White, 2000). In any case, integration of petrography, seismic stratigraphy and biostratigraphic data

evidence that these volcanoclastic rocks were: i) erupted in relatively deep-water depths (bathyal; ca 1000 to 1500 m), ii) experienced volcanic fragmentation processes (explosive or autoclastic), iii) may or may not have been reworked, and iv) were deposited in the cone apron of the volcano pc14 and near the ring plain of nf01, nf02 and nf03, which reinforces that both end members, primary and reworked volcanoclastics, could be present in the well (Figure 4).

XRF results indicate a bulk composition of ca 45% of silica (SiO_2), ca 14% of Al_2O_3, and contain Fe, Mg, K, Ca and Ti. SEM-EDS analyses in the volcanic glass show an average composition of ca 55% of silica (SiO_2), ca 17% of Al_2O_3 and contents of Fe, Mg, K, Ca, Ti and Na. These results are consistent with the analyses in the monzogabbro intrusion and also indicate a basaltic composition, and together with interpretation from seismic lines (e.g. Figure 17), reinforce a genetical correlation between both intrusive and extrusive rocks.

Age of the MVF and depth of the monzogabbro intrusion

To estimate the age of active volcanism in the MVF, we consider biostratigraphic data (Schiøler et al., 2011), a K-Ar date of the monzogabbro intrusion (Milne, 1975), sedimentological aspects of the strata that enclose both intrusive and volcanoclastics (e.g. amount of compaction and sedimentation rates), and results from seismic stratigraphic mapping (Figure 8; Figure 17). The oldest MVF volcanoclastic rocks (1220 m in Resolution-1) correlate to the transition from the Lillburnian to the lower Waiauan New Zealand stages (ca 12.7 Ma), thus, we assume an onset of MVF volcanism at 12.7 Ma (Figure 8). The youngest volcanoclastics occur at 1103.5 m in the well, however, there is no direct biostratigraphic age correlation at this depth (Figure 8). To define the end of MVF volcanic activity, we calculate the sedimentation rates of the middle and upper Tokama, from the depth interval between 1255 and 1030 m in the

well (Figure 8). The difference in thickness and age on this interval are 215 m and 2.59 Ma, respectively. To reduce the effect of the thickness of volcanic rocks on sedimentation rates, we subtract 10 m, which was estimated from the density and gamma logs in the well (Figure 8). This gives us an average sedimentation rate of 83 m/Ma (or 0.0120 Ma/m). Assuming that the sedimentation rate was constant, we multiply the siltstone thickness of the MVF interval (106.5 m) per calculated sedimentation rate (0.0120 Ma/m), which suggests that MVF was active for ca 1.2 Ma. Thus, the estimated onset of MVF volcanism (12.7 Ma) minus its calculated active time, suggest that the cessation of volcanism in the MVF was around 11.5 Ma, which is consistent with the K-Ar age of crystallization of the intrusion (12 ± 2 Ma; Milne, 1975).

To estimate the depth of emplacement of the monzogabbro penetrated by Resolution-1, we first subtract the depth of the surface marking the onset of volcanism in the MVF (1220 m in the well), from the depth of the intrusion (1911.5 m in the well), which produces a difference of 691.5 m. Next, we assume constant compaction for these sedimentary pile of 40%, which is based on compaction curves for sediments in the Canterbury Basin presented in Field et al. (1989). These calculations give us an emplacement depth of ca 968.1 m below the contemporary paleo sea-bed, which is consistent with petrographic observations that suggest a shallow level intrusion for the monzogabbro.

Conclusions

Rock samples collected by the petroleum exploration well Resolution-1 evidence that submarine volcanic eruptions and shallow magmatic intrusions occurred in the Canterbury Basin during the middle Miocene. Biostratigraphic data and K-Ar dating suggest that this magmatism was active from ca 12.7 to 11.5 Ma. The magmatic

products are primarily mafic in composition. XRF, SEM-EDS and petrographic analysis suggest a co-genetic correlation between both intrusive and volcanoclastic rocks. This correlation is reinforced by seismic reflection imagery of a saucer-shaped sill (i.e. monzogabbro) that likely fed volcanic eruptions (i.e. volcanoclastics) onto the middle Miocene paleo-seafloor at the location of the Resolution-1. Miarolitic cavities and ophitic texture observed in the monzogabbro suggest that the saucer-shaped sill was injected at shallow depths, which is estimated to be around 950 m below the paleo-surface at the time of the intrusion. The host rocks were affected by hydrothermal alteration, which is evident in carbonate veins and abundant zeolites cross-cutting paralic to neritic rocks, and by the presence of microfossils showing an increasing degree of thermal alteration towards the intrusion. Petrographic, wire-line logs and biostratigraphic analysis of the well indicate that the eruption occurred in a lower bathyal setting (1000 -1500 m depth). Due to limitations of interpreting data from well-cuttings, it was not possible to precisely determine the eruptive-styles that formed the volcanoclastic rocks. However, the high content of shards of glass, relics of bubble walls, presence of spheroidal aggregates (armoured lapilli), fragments enveloped in palagonite films, and broken phenocrysts, suggests submarine explosivity and subsequent flow transportation and deposition in the area of the Resolution-1 well. In the second part of this study, we progressively up-scale interpretations to a regional scale, based on seismic stratigraphic mapping techniques, presenting the seismic morphological reconstruction of the volcanoes on the MVF. The integration of the results from petrographic and seismic reflection analysis allows us to interpret the eruptive-styles and degradation processes that formed and modified these volcanoes now “fossilized” in the Canterbury Basin.

Table 1: Main stratigraphic and paleoenvironmental characteristics of the Tokama Siltstone depositional units. Highlighted middle Tokama unit (red) is interbedded with the volcanoclastic rocks described in section “Volcanoclastic Rocks”.

Depositional unit	Depth in the well	Age	Depositional setting	Lower bound	Upper bound	Thickness (m)
Uppermost Tokama	1016 to 686.1	Late early Miocene to late Pliocene	Uppermost bathyal	Unc. lM	Unc. eP	329.9
Upper Tokama	1070 to 1016	Late early Miocene	Mid bathyal	Onset of slope progradation	Unc. lM	54
Middle Tokama	1269 to 1070	Middle Miocene	Lower bathyal (1500-1000 m)	Unc. eM	Onset of slope progradation	190
Lower Tokama	1284.1 to 1269	late early Miocene	deep lower bathyal	Omihi Fm	Unc. eM	24

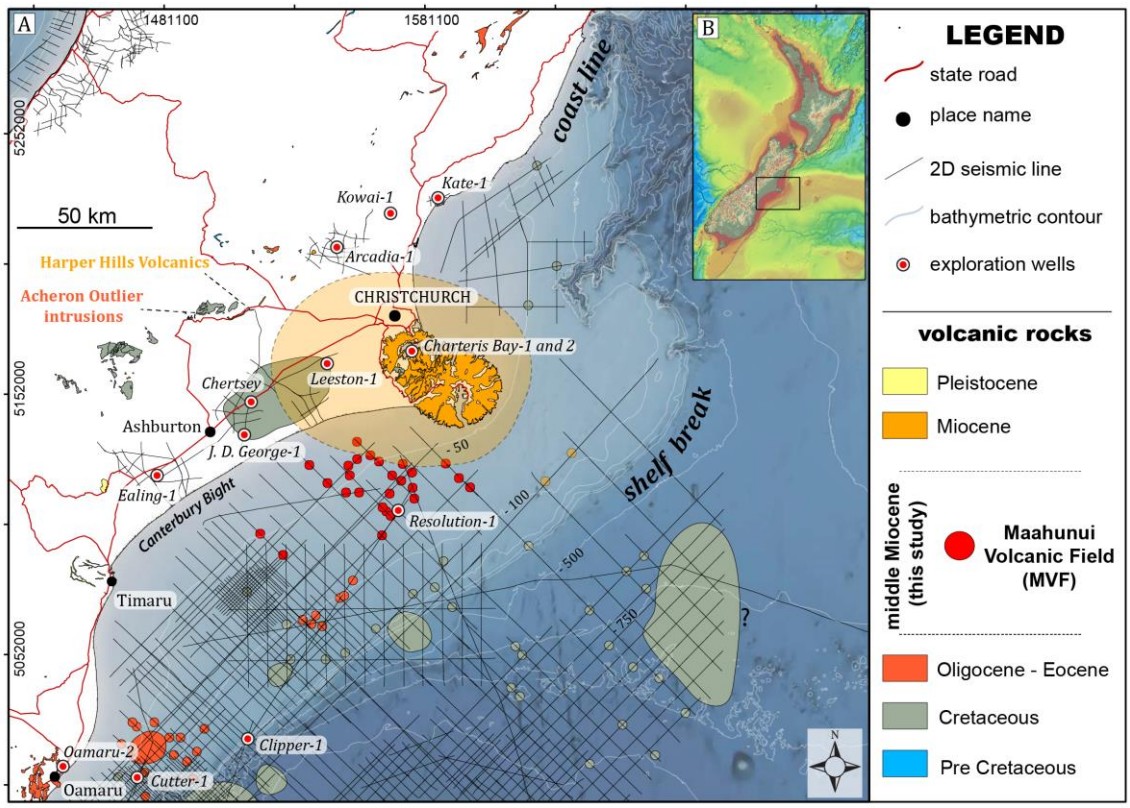

Figure 1: A) Map showing the age and location of volcanic rocks onshore and offshore northern Canterbury Basin, together with the main seismic and well data used in this work. Red dots indicate the locations of volcanoes in the Maahunui Volcanic Field, which is the focus of this study. Onshore volcanoes are from GNS geologic map (Forsyth et al., 2008). B) New Zealand topographic and bathymetric map from the NZ Petroleum Exploration 2018 datapack. Black square in B) shows the location of the detailed map in A.

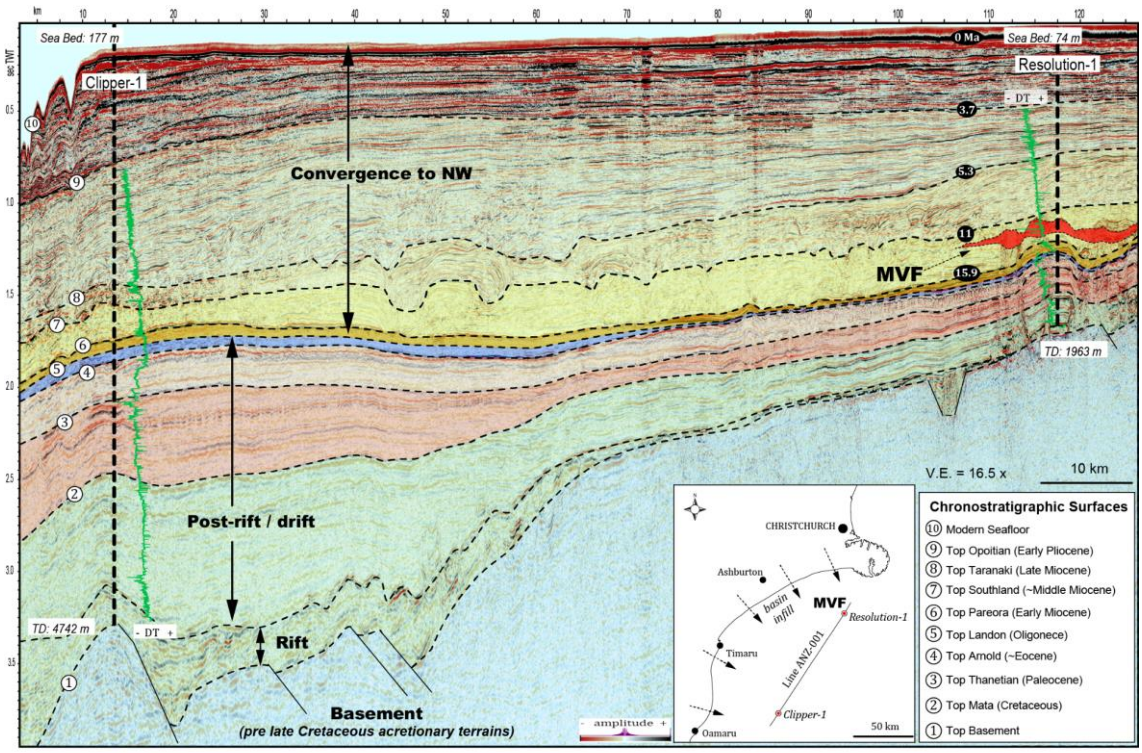

Figure 2: 2D regional strike/oblique seismic line showing the stratigraphic architecture, the main geotectonic events in the northern part of the Canterbury Basin, and the location of the MVF (red). The Resolution-1 and Clipper-1 wells were used to tie the seismic data to chronostratigraphic surfaces that represent important changes during the basin evolution.

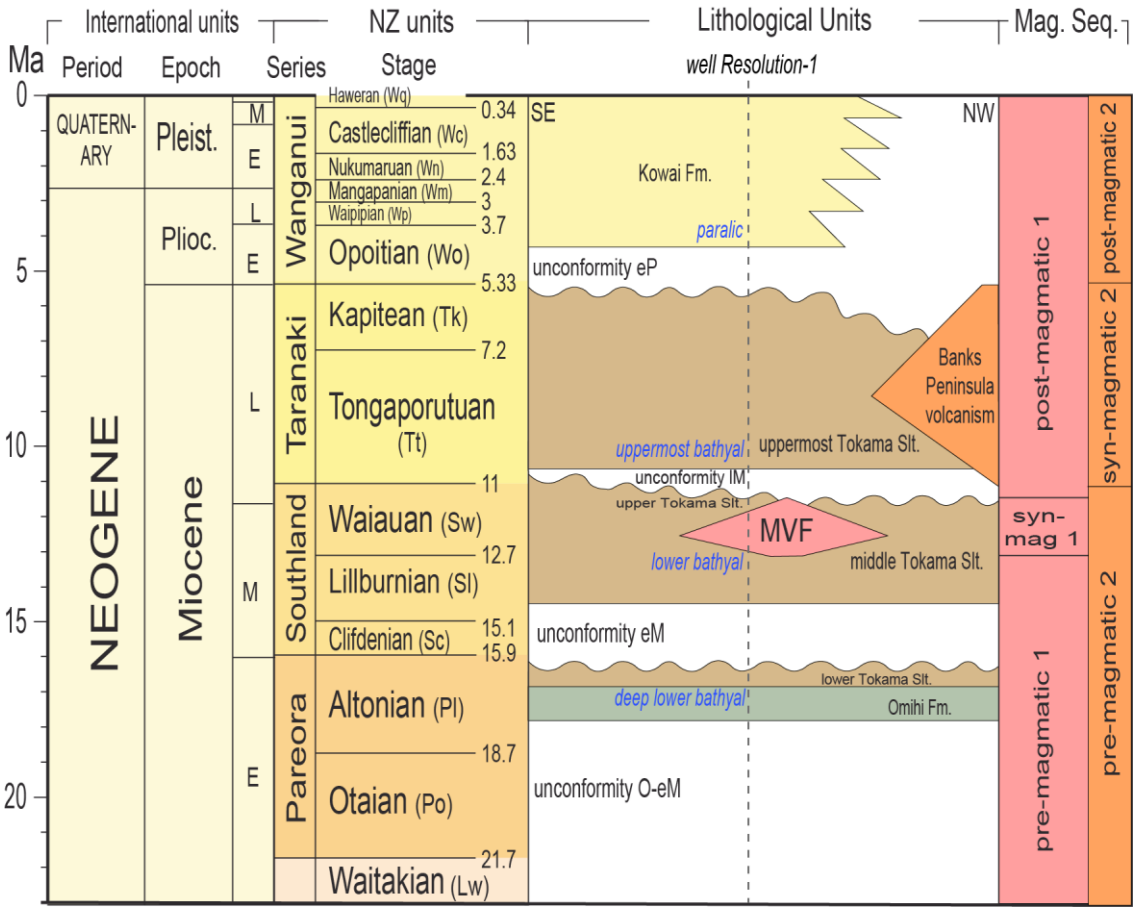

Figure 3: Local chronostratigraphic chart of the study area. We subdivide Tokama Siltstone (black label) within the vicinity of MVF into four depositional units according to their depositional setting (blue italic label). Two main volcanic events within northern Canterbury basin during the Miocene emplaced MVF and Banks Peninsula. The main magmatic events are each represented by pre, syn and post-magmatic sequences, and are shown in the right part of the figure. Magmatism in pink is related with MVF, while in orange is related with Banks Peninsula. Stratigraphic ages follow the International Chronostratigraphic Chart 2014 and New Zealand Geological Time Scale 2015 (Raine et al., 2015).

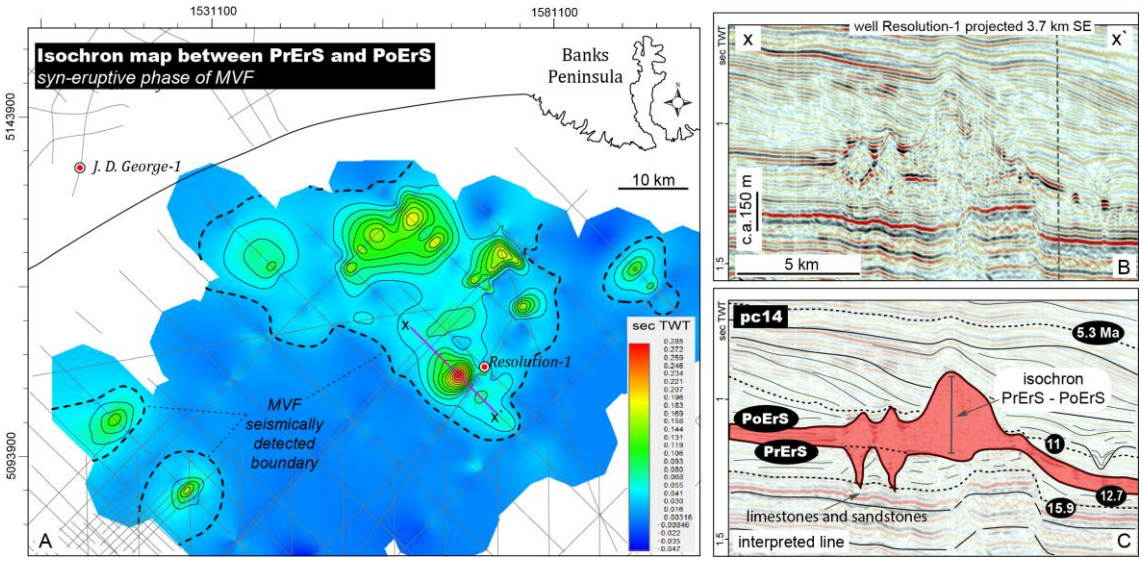

Figure 4: A) Isochron map between pre-eruptive (PrErS) and post-eruptive surfaces (PoErS) of MVF showing the location of MVF cone-type volcanoes. Note that the surfaces thin and amalgamate with increasing distance from individual or clusters of volcanoes, defining the seismic detectable boundaries of MVF. B) Uninterpreted seismic section across volcano pc-14. C) Interpretation of seismic section in (B) showing the PrErS and PoErS surfaces and the associated isochron. Diatremes were excluded during mapping of the PrErS surface due to computer limitations, as they would have shown a false positive structure in the isochron map.

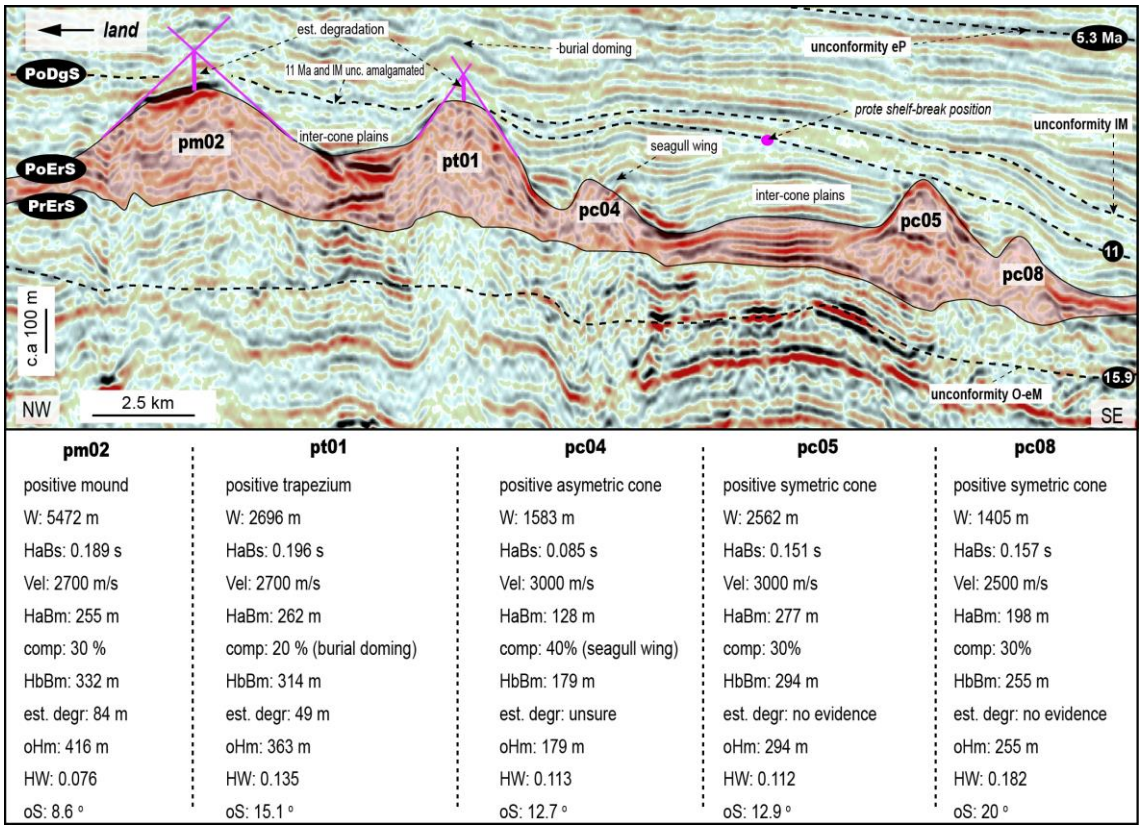

pm02	pt01	pc04	pc05	pc08
positive mound	positive trapezium	positive asymetric cone	positive symetric cone	positive symetric cone
W: 5472 m	W: 2696 m	W: 1583 m	W: 2562 m	W: 1405 m
HaBs: 0.189 s	HaBs: 0.196 s	HaBs: 0.085 s	HaBs: 0.151 s	HaBs: 0.157 s
Vel: 2700 m/s	Vel: 2700 m/s	Vel: 3000 m/s	Vel: 3000 m/s	Vel: 2500 m/s
HaBm: 255 m	HaBm: 262 m	HaBm: 128 m	HaBm: 277 m	HaBm: 198 m
comp: 30 %	comp: 20 % (burial doming)	comp: 40% (seagull wing)	comp: 30%	comp: 30%
HbBm: 332 m	HbBm: 314 m	HbBm: 179 m	HbBm: 294 m	HbBm: 255 m
est. degr: 84 m	est. degr: 49 m	est. degr: unsure	est. degr: no evidence	est. degr: no evidence
oHm: 416 m	oHm: 363 m	oHm: 179 m	oHm: 294 m	oHm: 255 m
HW: 0.076	HW: 0.135	HW: 0.113	HW: 0.112	HW: 0.182
oS: 8.6 °	oS: 15.1 °	oS: 12.7 °	oS: 12.9 °	oS: 20 °

Figure 5: 2D dip section (line CB-82-06) showing evidence of differential degradation related with the late Miocene (lM) unconformity and of differential compaction (burial doming and “seagull wings”). PrErS is the pre-eruptive surface, while PoErS is the post-eruptive surface. PoDgS is the post-gradational surface.

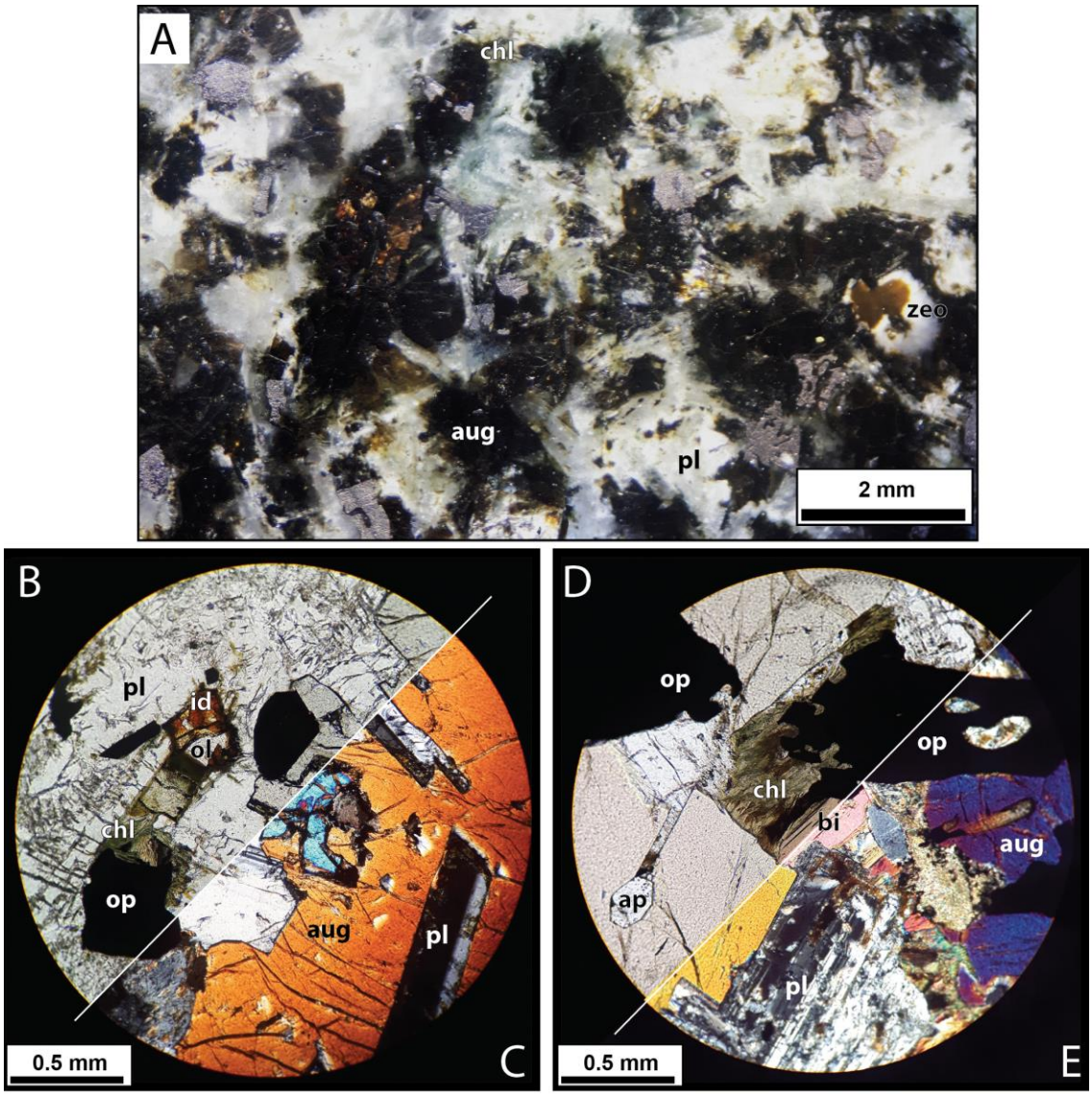

Figure 6: Macroscopic and microscopic photographs of the monzogabbro recovered from a depth of -1962.25 m in the Resolution-1 well. A) Photograph of a medium-grained leucocratic intrusive rock composed of plagioclase (pl) and pyroxene (aug). Zeolite analcite (zeo) occurs filling cavities. Chlorite (chl) occurs as an alteration of primary minerals. Thin-section photographs in plain (B and D) and cross-polarized light (C and E) showing ophitic texture of plagioclase (pl) and augite (aug), olivine (ol) crystals partially replaced by iddingsite (id), and clinopyroxenes (aug) replaced by biotite (bi) and chlorite (chl), which suggests magma crystallization at shallow depths and H2O interaction. Accessory minerals are opaques (op) and apatite (ap).

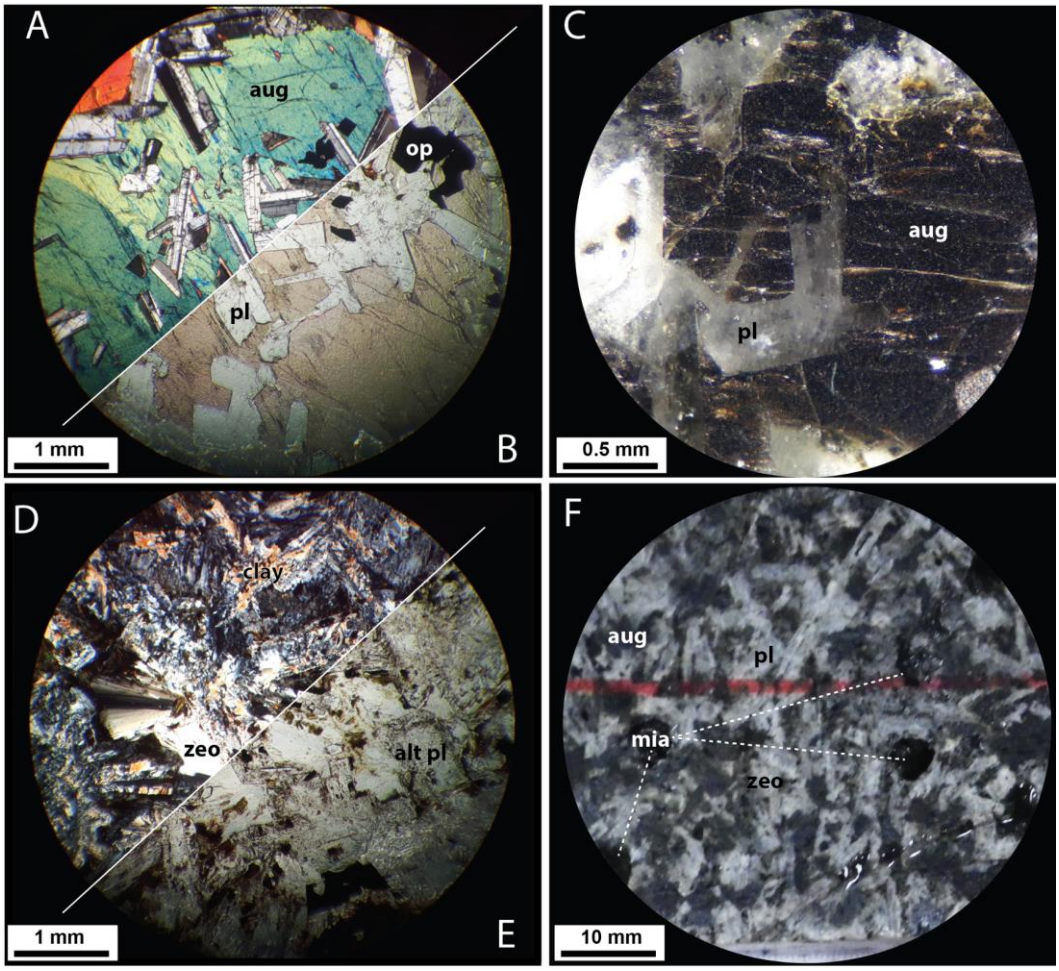

Figure 7: Macroscopic and microscopic photographs of the monzogabbro recovered at -1962.25 m in the well Resolution-1. Thin-section in cross-polarized light (A), plain light (B) and macroscopic polished section (C) showing augite (aug) and plagioclase (pl) with ophitic texture. Thin section in cross-polarized light (D) and natural light (E) showing zeolite (zeo) filling interstitial space and plagioclase altered to clays. Macroscopic photograph of Resolution-1 core at the depth of 1663 m (C) showing augite, plagioclase, acicular crystals of zeolite and miarolitic cavities (mia).

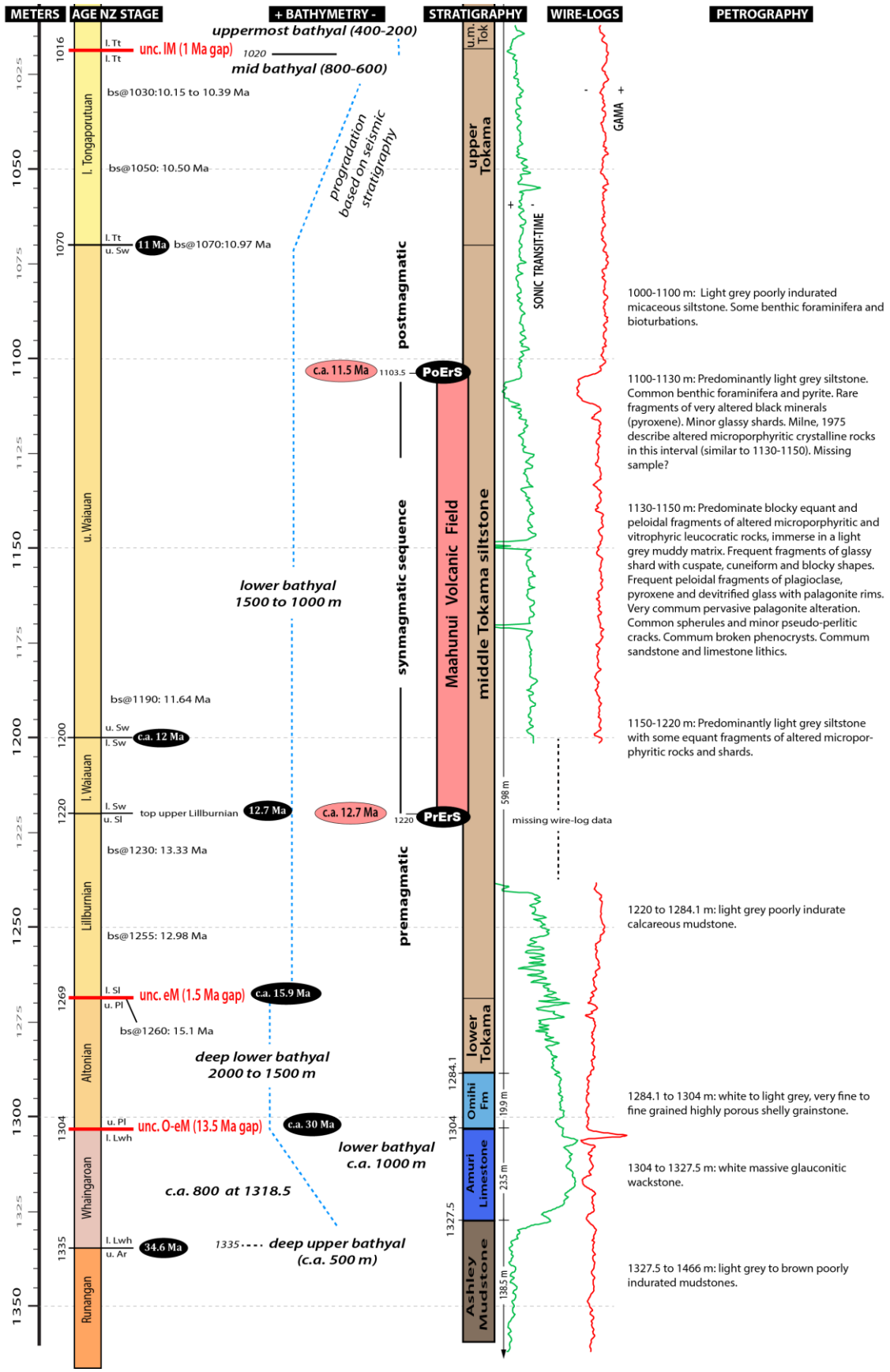
METERS
AGE NZ STAGE
+ BATHYMETRY -
STRATIGRAPHY
WIRE-LOGS
PETROGRAPHY
uppermost bathyal (400-200)
mid bathyal (800-600)
unc. lM (1 Ma gap)
bs@1030:10.15 to 10.39 Ma
bs@1050: 10.50 Ma
11 Ma
bs@1070:10.97 Ma
progradation based on seismic stratigraphy
postmagmatic
c.a. 11.5 Ma
PoErS
synmagmatic sequence
Maahunui Volcanic Field
middle Tokama siltstone
lower bathyal 1500 to 1000 m
bs@1190: 11.64 Ma
c.a. 12 Ma
top upper Lillburnian
12.7 Ma
c.a. 12.7 Ma
PrErS
premagmatic
bs@1230: 13.33 Ma
bs@1255: 12.98 Ma
unc. eM (1.5 Ma gap)
c.a. 15.9 Ma
bs@1260: 15.1 Ma
deep lower bathyal 2000 to 1500 m
unc. O-eM (13.5 Ma gap)
c.a. 30 Ma
lower bathyal c.a. 1000 m
c.a. 800 at 1318.5
34.6 Ma
deep upper bathyal (c.a. 500 m)
upper Tokama
lower Tokama
Omihi Fm
Amuri Limestone
Ashley Mudstone
SONIC TRANSIT-TIME
GAMA
598 m
missing wire-log data
199 m
235 m
138.5 m
1000-1100 m: Light grey poorly indurated micaceous siltstone. Some benthic foraminifera and bioturbations.
1100-1130 m: Predominantly light grey siltstone. Common benthic foraminifera and pyrite. Rare fragments of very altered black minerals (pyroxene). Minor glassy shards. Milne, 1975 describe altered microporphyritic crystalline rocks in this interval (similar to 1130-1150). Missing sample?
1130-1150 m: Predominate blocky equant and peloidal fragments of altered microporphyritic and vitrophyric leucocratic rocks, immerse in a light grey muddy matrix. Frequent fragments of glassy shard with cuspate, cuneiform and blocky shapes. Frequent peloidal fragments of plagioclase, pyroxene and devitrified glass with palagonite rims. Very commum pervasive palagonite alteration. Common spherules and minor pseudo-perlitic cracks. Commum broken phenocrysts. Commum sandstone and limestone lithics.
1150-1220 m: Predominantly light grey siltstone with some equant fragments of altered micropor-phyritic rocks and shards.
1220 to 1284.1 m: light grey poorly indurate calcareous mudstone.
1284.1 to 1304 m: white to light grey, very fine to fine grained highly porous shelly grainstone.
1304 to 1327.5 m: white massive glauconitic wackstone.
1327.5 to 1466 m: light grey to brown poorly indurated mudstones.
l. Tongaporutuan
u. Waiauan
l. Waiauan
Lillburnian
Altonian
Whaingaroan
Runangan

Figure 8: Composite data of the Oligocene-Miocene interval of Resolution-1 well showing the lithologies, ages, paleoenvironments, stratigraphy, and wire-logs. Symbol bs@ is the given biostratigraphic age in Schiøler et al. (2011). Blue dashed lines show the bathymetry trend. Numbers in black ellipses are ages according to the 2015 NZ Geologic Time Scale (Raine et al., 2015). Numbers in red ellipses are estimated ages of the MVF based on the integration of this dataset.

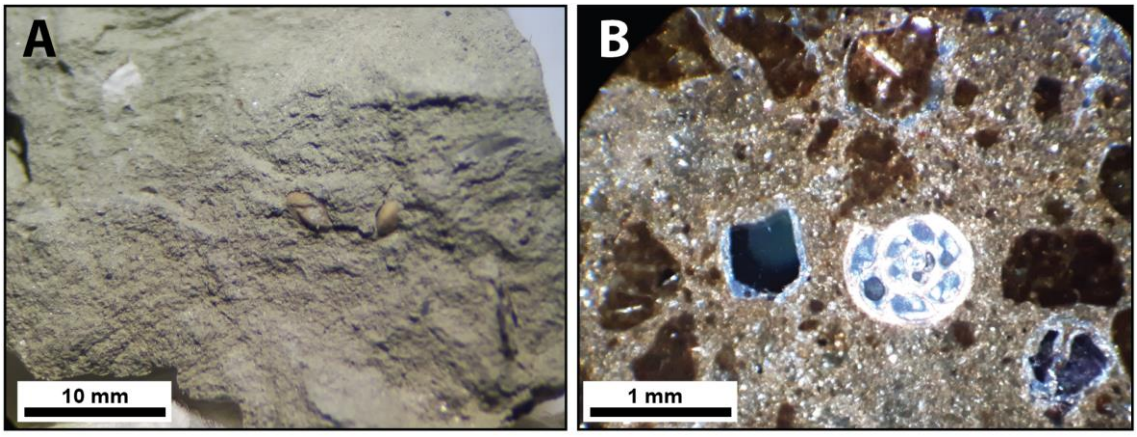

Figure 9: A) Macroscopic photograph of an unwashed cuttings sample of massive siltstone containing benthonic foraminifera recovered from the interval 1120 to 1130 m from the Resolution-1 well (middle Tokama). B) Microscope photograph in crossed-polarized light of unwashed cutting samples of volcanic clasts and a gastropod in a muddy matrix from the interval of 1130 to 1140 m in Resolution-1.

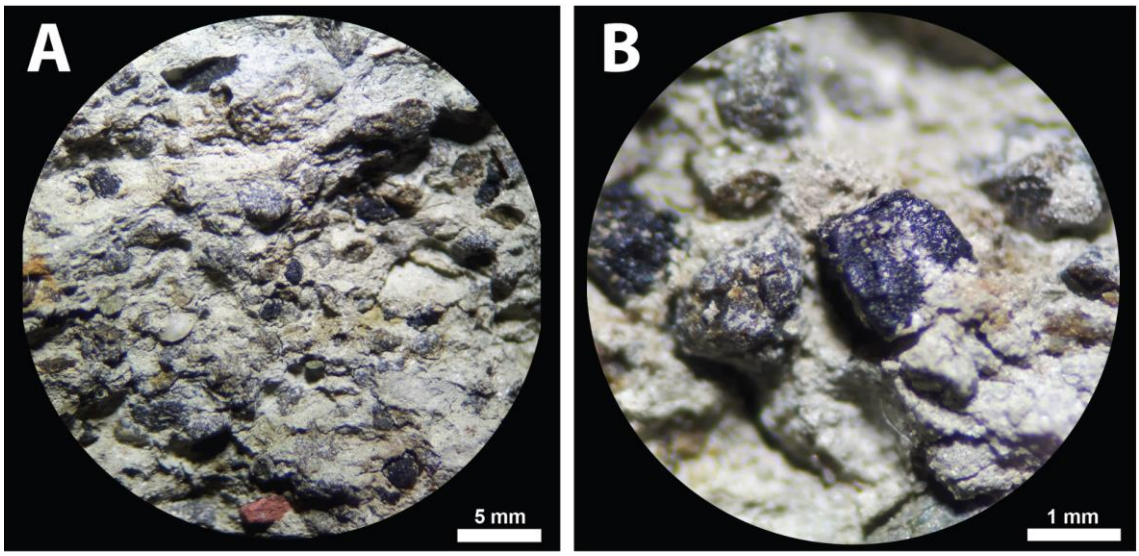

Figure 10: Macroscopic photographs of unwashed cutting samples from the interval of -1130 to -1140 m in Resolution-1. A) Volcanic fragments and bioclasts immersed in a muddy matrix. Black fragments are mainly altered pyroxenes (B).

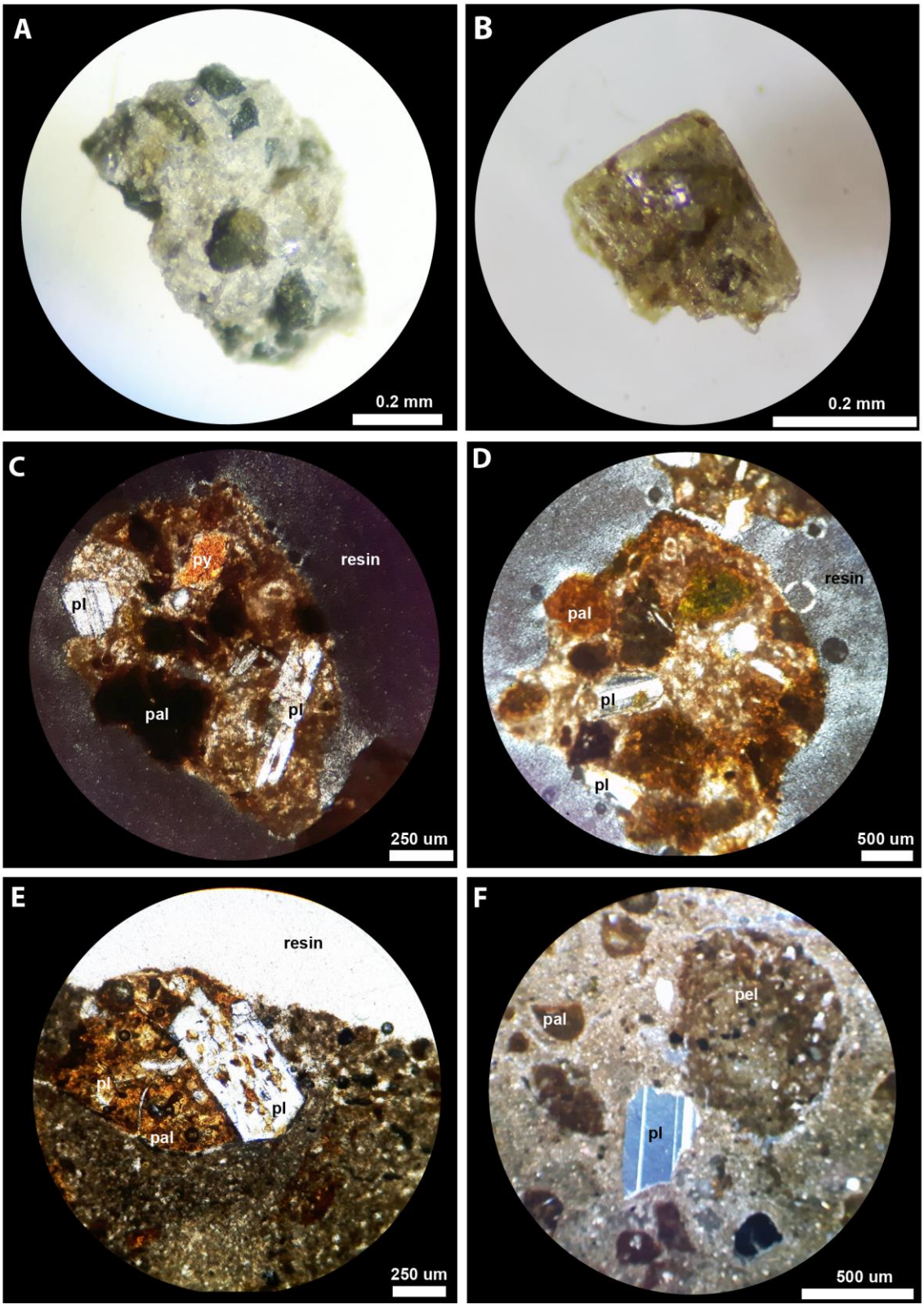

Figure 11: Macroscopic photographs of plagioclase (pl) and pyroxene (py) phenocrysts in microporphyritic texture (A), and a broken plagioclase fragment (B). C to F show photographs in cross-polarized thin-section of rocks with microporphyritic and

vitrophyric textures. Note that phenocrysts with broken angular borders (C and F) are associated with peloidal (pel) and palagonite (pal) clasts.

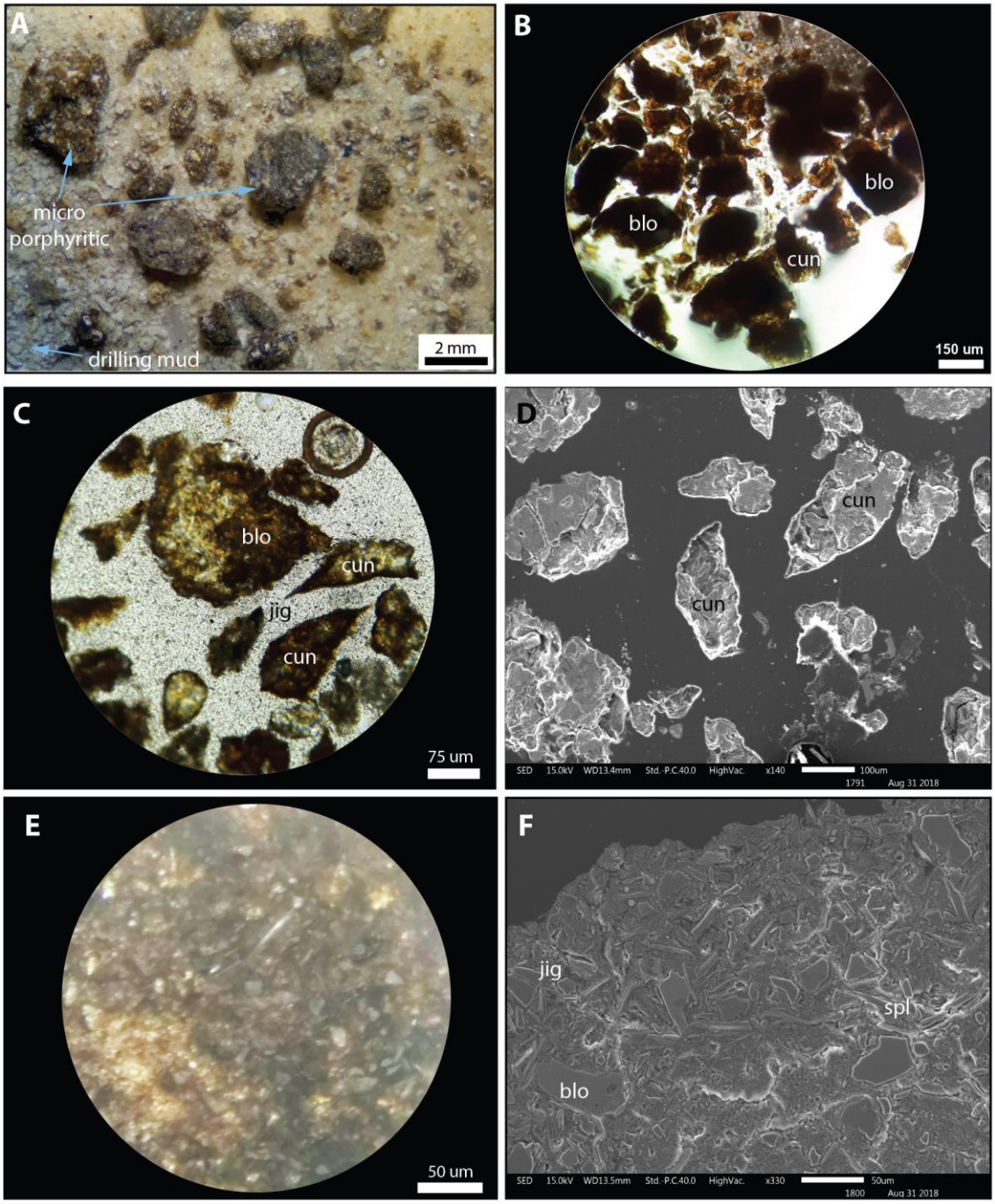

Figure 12: Macroscopic images of volcanic fragments submerged in water (A) during the washing process of samples from the interval of -1130 to -1140 m in Resolution-1. These rocks show altered microporphyritic texture with blocky equant and jigsaw-fit texture. Microscope (B and C) and SEM (D) images of spall shards with cuneiform

(cun), and blocky (blo) shapes in jigsaw-fit (jig) texture. Microscope (E) and SEM (F) images of loose glassy shards with blocky and splintery (spl) shapes in vitriclastic and jigsaw-fit jig texture.

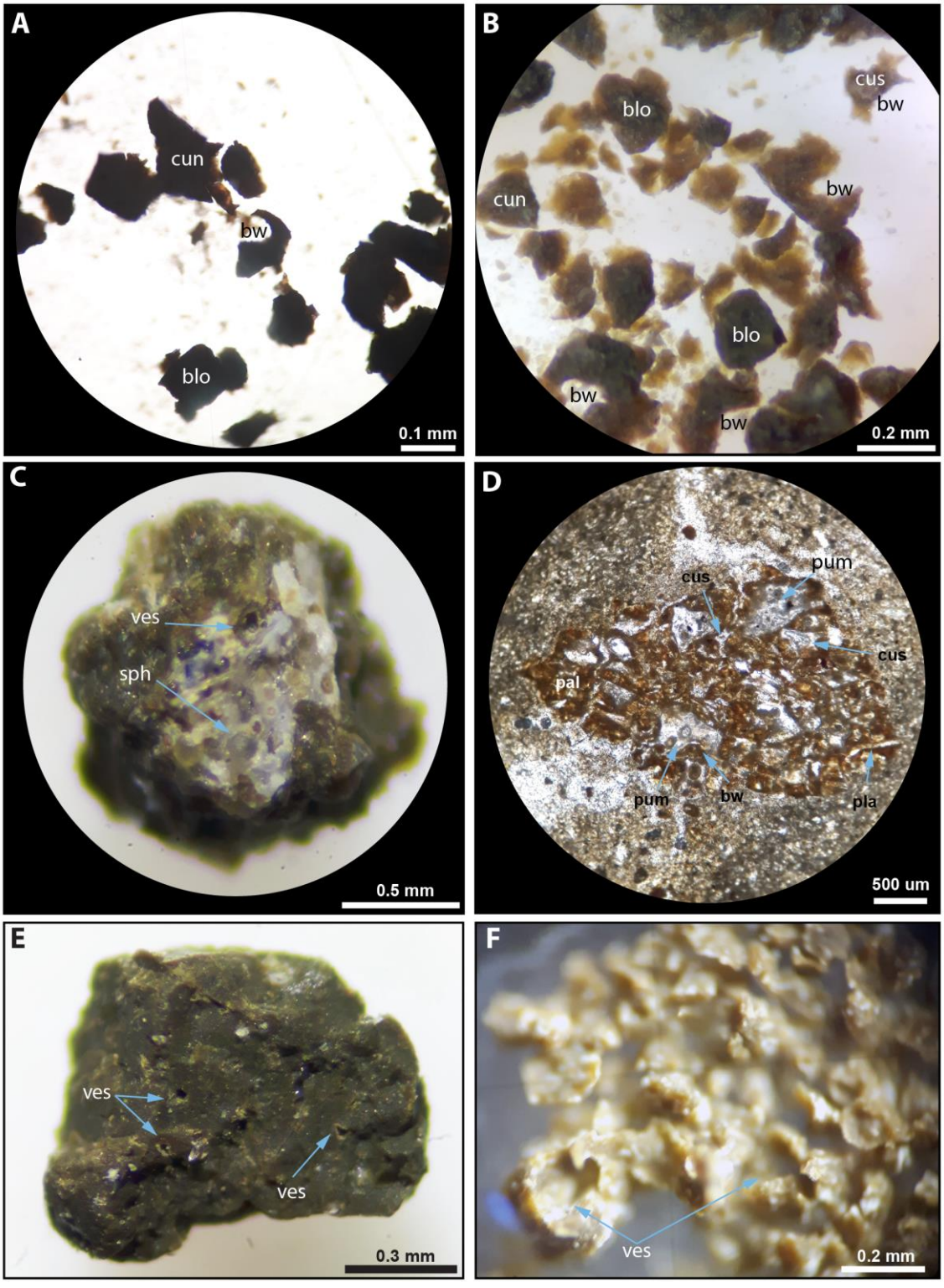

Figure 13: A and B) Macroscopic images of loose shards with cuspate, cuneiform, blocky (blo) and platy (pla) shapes, and common relic bubble walls (bw). C) Hypocrystalline fragment containing concentric spherules (sph) and vesicles (ves). D) Photograph of thin-sections in plain light showing palagonite (pal) and glassy shards with, cuspate (cus), platy (pla) and pumice (pum) shapes, and relics of bubble walls (bw). E) Macroscopic image of microcrystalline blocky equant fragment with some micro-vesicles. F) Macroscopic photograph of loose and poorly indurated spalls of shards with common vesicles.

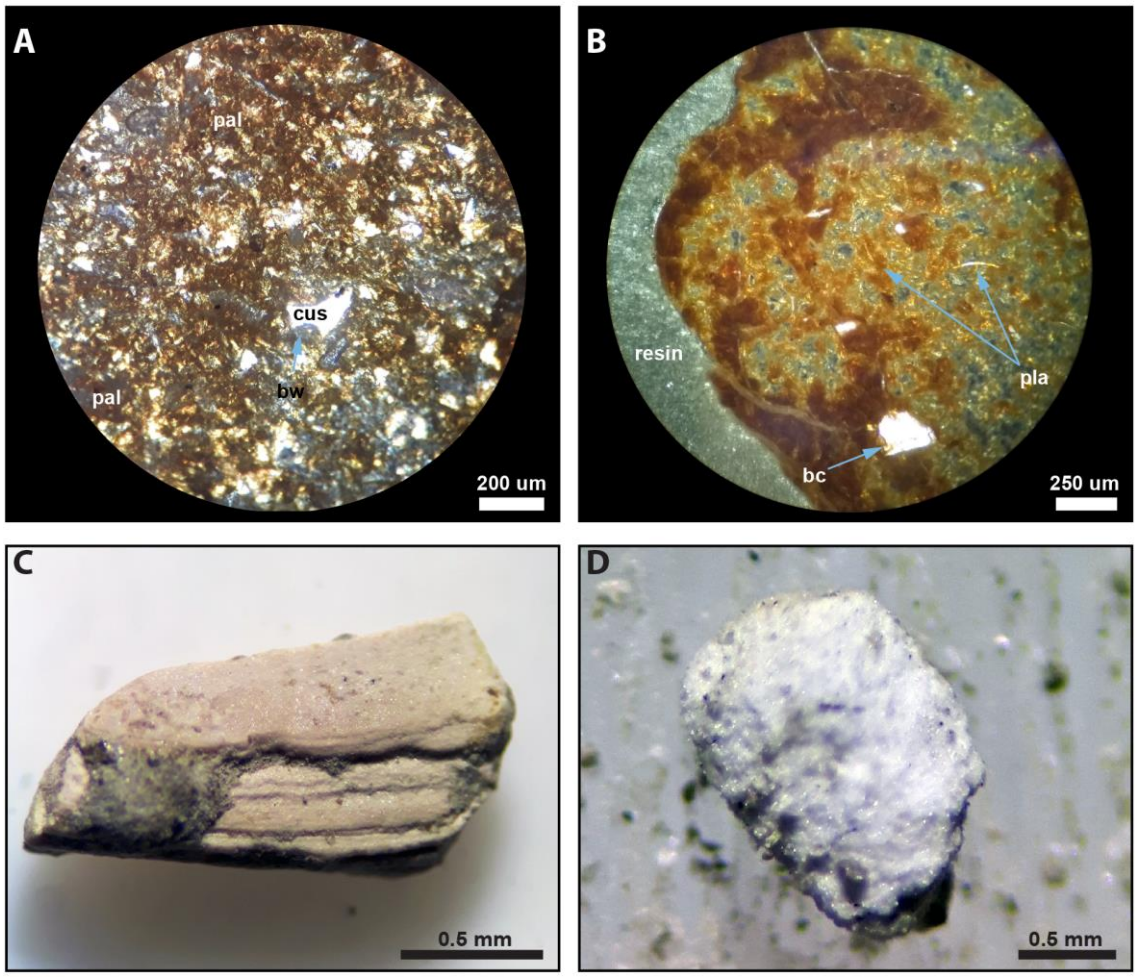

Figure 14: A and B) Thin-sections in plain light showing fragments of very-fine grained rocks with a pervasive alteration to palagonite (pal), shards with cuspate (cus) and platy (pla) shapes, and fragments of broken crystals (bc). Macroscopic images of limestone (C) and sandstone lithics (D), which may correspond to rocks of Amuri and Omihi limestones, and Charteris Bay sandstone.

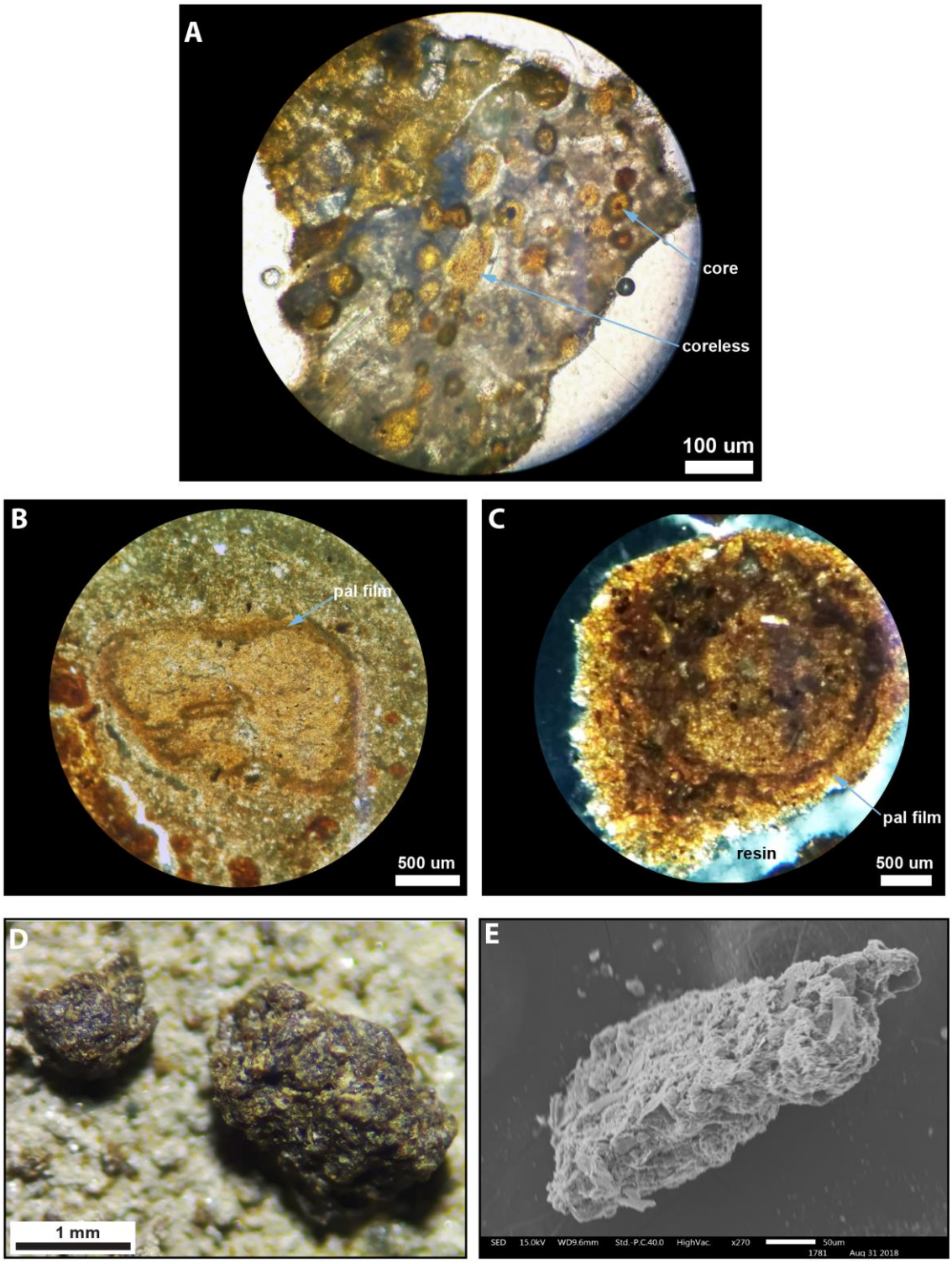

Figure 15: Thin-sections in plain (A and B) and cross-polarized (C) light showing spherules with and without an inner core enveloped in a palagonite (pal) film. Macroscopic (D) and SEM (E) examples of poorly indurated highly porous glassy aggregate are also displayed.

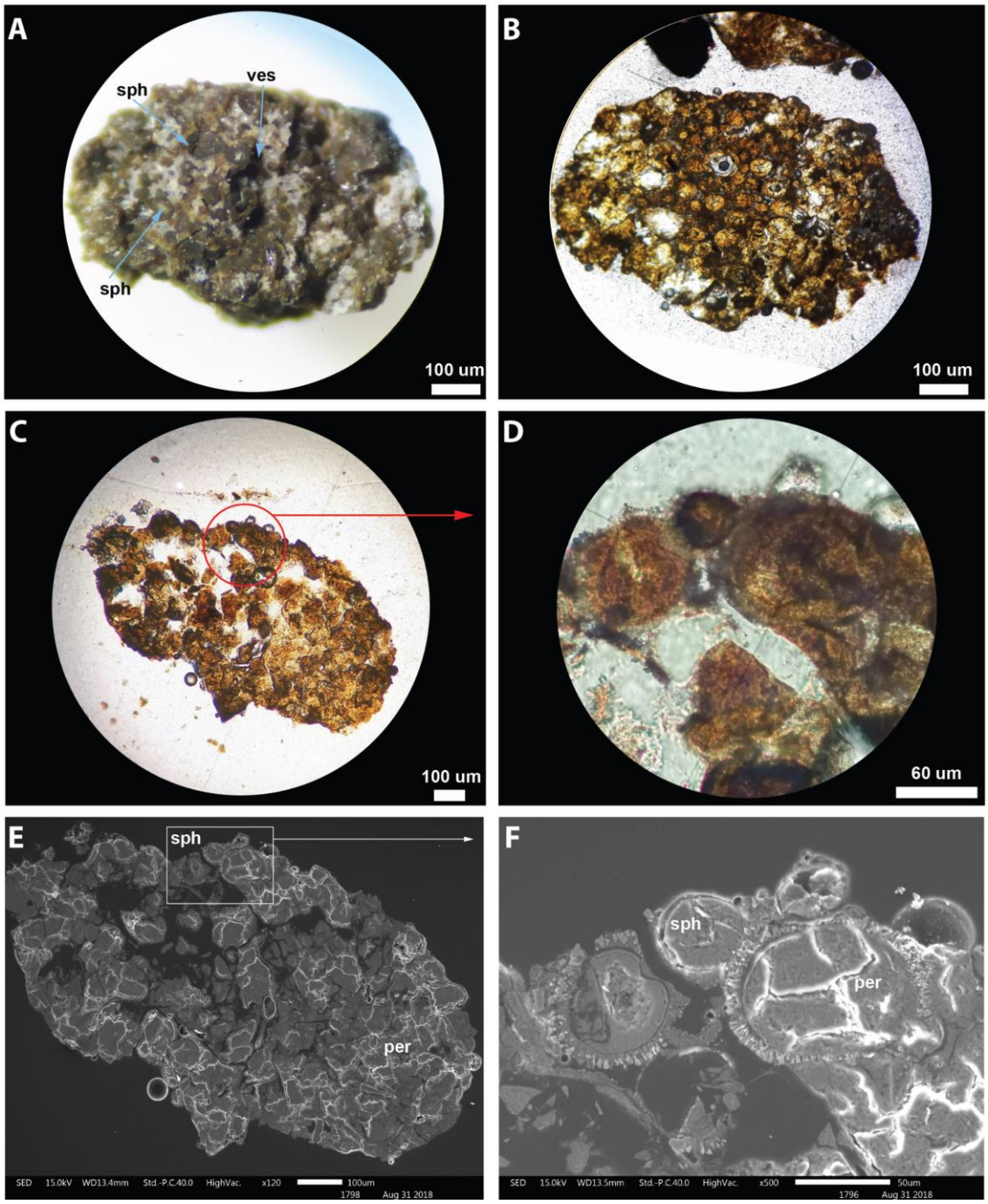

Figure 16: Macroscopic (A) and plain light microscopic (B) examples of well indurated aggregate of cored spherules (sph), associated with vesicles (ves) and intense palagonite alteration. Plain light (B), cross-polarized and SEM (E and F) images of spherule with a glassy devitrified (palagonite) inner core, enveloped in a single concentric outer rim associated with an array of acicular crystals in radial pattern and pseudo-perlitic (per) cracks.

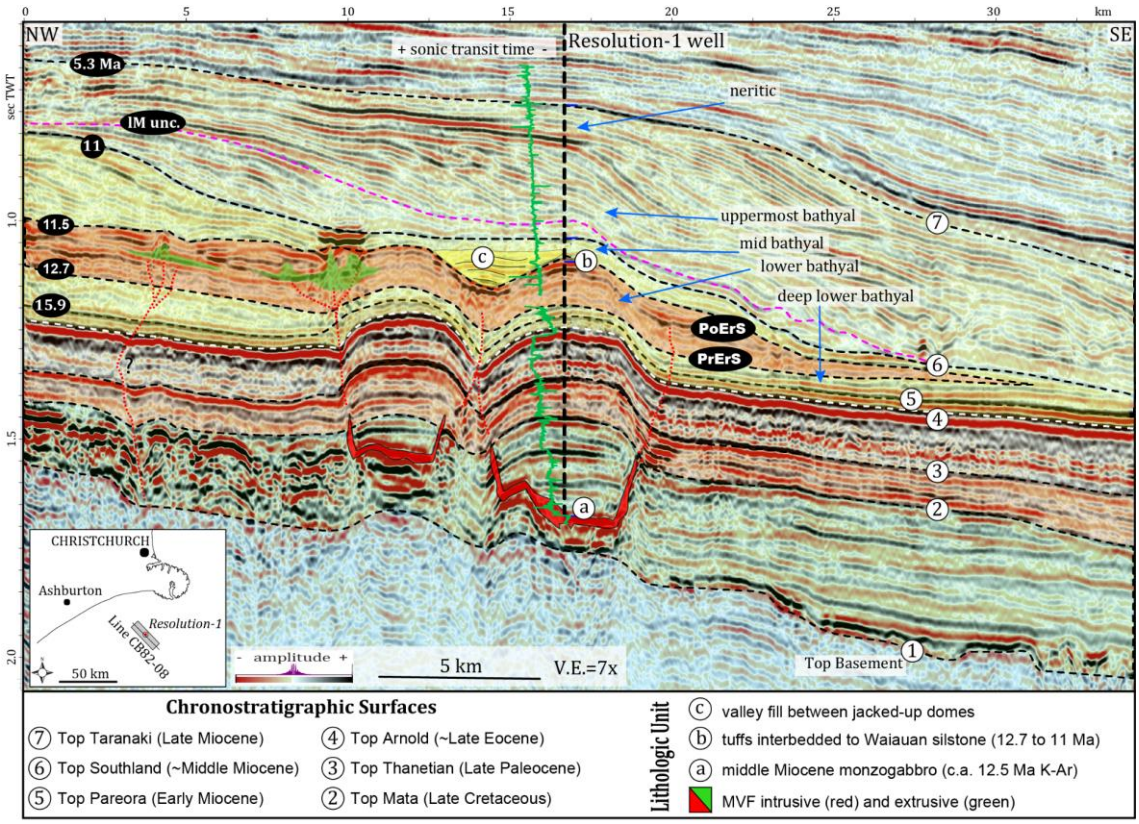

Figure 17: Interpreted 2D dip seismic section at the Resolution-1 well (thick dashed line). Saucer-shaped sills (a) were intruded into Cretaceous sedimentary strata during the middle Miocene (ca 12.5 Ma K-Ar) and caused doming of the overlying strata. The doming consequentially changed the Waiauan paleo-sea floor topography and promoted deposition as channelized systems of lower Tongaporutuan age (c) next to the dome structures. The syn-eruptive interval (between PrErS and PoErS) is defined by the occurrence of volcanic material (b) interbedded with sedimentary rocks of the Tokama Siltstone of Waiauan age (ca 12.7 to 11 Ma) and seismic stratigraphic analysis. At the border of the domed strata, disrupted reflectors and faults suggest magma and hydrothermal fluid pathways that fed eruptions onto the middle Miocene paleo-seafloor. The available evidence together with geochemical and petrographic analysis demonstrate that the intrusive and extrusive rocks penetrated by the Resolution-1 well likely have a co-genetic relationship, which together with estimations of sedimentation rate in the area allow us to propose that the MVF was formed from ca 12.7 to 11.5 Ma.

References

Aarnes, I., Planke, S., Trulsvik, M., Svensen, H., 2015. Contact metamorphism and thermogenic gas generation in the Vøring and Møre basins, offshore Norway, during the Paleocene-Eocene thermal maximum. Journal of the Geological Society, 172(5), 588-598.

Abdelmalak, M. M., S. Planke., J. I. Faleide., D. A. Jerram., D. Zastrozhnov., S. Eide., R. Myklebust., 2016, The development of volcanic sequences at rifted margins: New insights from the structure and morphology of the Vøring Escarpment, mid-Norwegian Margin: Journal of Geophysical Research, Solid Earth, 121, 5212–5236, https://doi.org/10.1002/2015JB012788

Agirrezabala, L., Sarrionandia, F., Carracedo, M., 2017, Diatreme-forming volcanism in a deep-water faulted basin margin: Lower Cretaceous outcrops from the Basque-Cantabrian Basin, western Pyrenees. Journal of Volcanology and Geothermal Research. https://doi.org/10.1016/j.jvolgeores.2017.03.019

Arnórsson, S., S. Thórhallsson., A. Stefánsson., 2015, Utilization of Geothermal Resources, in The Encyclopedia of Volcanoes: https://doi.org/10.1016/B978-0-12-385938-9.00071-7

Ballance, P.F., 1993, The New Zealand Neogene forearc basins, in Ballance, P.F., ed., South Pacific Sedimentary Basins, Sedimentary Basins of the World 2: Amsterdam, Elsevier Science, p. 177–193.

Barrier,.A., A. Nicol, A. P. Bischoff., 2017, Volcanism Occurrences in the Canterbury Basin, New Zealand and Implication for Petroleum Exploration. In AAPG GTW Influence of Volcanism and Associated Magmatic Processes on Petroleum Systems. Conference, Oamaru New Zealand.

Batt, G. E., S. L. Baldwin., M. A, Cottam., P. G, Fitzgerald., M. T, Brandon., T. L. Spell., 2004, Cenozoic plate boundary evolution in the South Island of New Zealand: New thermochronological constraints: Tectonics, https://doi.org/10.1029/2003TC001527

Best, M. G., E. H. Christiansen., 1997, Origin of broken phenocrysts in ash-flow tuffs: Bulletin of the Geological Society of America, https://doi.org/10.1130/0016-7606(1997)109<0063:OOBPIA>2.3.CO;2

Bischoff, A.P., A. Nicol, A. Barrier, M. Beggs., 2016, The Stratigraphic Record of Volcanism - Examples from New Zealand Sedimentary Basins. In 2016 Geoscience Society of New Zealand Conference, Wanaka, Abstract.

Bischoff, A. P., A. Nicol, M. Beggs., 2017, Stratigraphy of architectural elements in a buried volcanic system and implications for hydrocarbon exploration: Interpretation, https://doi.org/10.1190/INT-2016-0201.1

Bischoff, A.P., 2019, Architectural Elements of Buried Volcanic Systems and Their Impact on Geoenergy Resources. Ph.D. Thesis, Canterbury University, New Zealand. Pre-print, 226p. doi: 10.13140/RG.2.2.21440.58886

Blanke, S. J., 2010, "Saucer Sills" of the Offshore Canterbury Basin: GNS Publication, https://doi.org:10.1177/0094306114545742f

Browne, G. H., 1983, A new interpretation of brecciation in the sandpit tuff, harper hills, Canterbury: New Zealand Journal of Geology and Geophysics, https://doi.org/10.1080/00288306.1983.10422258

Carlson, J. R., J. A. Grant-Mackie., K. A. Rodgers., 1980, Stratigraphy and sedimentology of the coalgate area, canterbury, new zealand: New Zealand Journal of Geology and Geophysics, https://doi.org/10.1080/00288306.1980.10424205

Cas, R. A. F., J. V. Wright., 1993, Volcanic Successions: Modern and Ancient - A Geological Approach to Processes, Products and Successions. Chapman and Hall, UK. https://doi.org:10.1007/978-0-412-44640-5

Cas, R. A. F., G. Giordano., 2014, Submarine volcanism: A review of the constraints, processes and products, and relevance to the Cabo de Gata volcanic succession: https://doi.org:10.3301/IJG.2014.46

Catuneanu, O., 2006, Principles of Sequence Stratigraphy. Changes, 375. https://doi.org:10.5860/CHOICE.44-4462

Coombs, D. S., A. J. R. White., D. Hamilton., and R. A. Couper., 1960, Age relations of the Dunedin volcanic complex and some paleogeographic implications—Part II: New Zealand Journal of Geology and Geophysics, https://doi.org:10.1080/00288306.1960.10420145

Coombs, D.S., Cas, R.A., Kawachi, Y., Landis, C.A., McDonough, W.F., Reay, A., 1986, Cenozoic volcanism in north, east and central Otago. In: Smith, I.E.M. (Ed.), Late Cenozoic Volcanism in New Zealand. R. Soc. N.Z. Bull. 23, pp. 278-312.

Delmelle, P., E. Maters., C. Oppenheimer., 2015, Volcanic Influences on the Carbon, Sulfur, and Halogen Biogeochemical Cycles, in The Encyclopedia of Volcanoes: https://doi.org/10.1016/B978-0-12-385938-9.00050-X

Deardorff, N. D., K. V. Cashman., W. W. Chadwick., 2011, Observations of eruptive plume dynamics and pyroclastic deposits from submarine explosive eruptions at NW Rota-1, Mariana arc: Journal of Volcanology and Geothermal Research, http https://doi.org/10.1016/j.jvolgeores.2011.01.003

Eady, A. E., 1995, The Petrology and Geochemistry of the Acheron Intrusion. Thesis, Canterbury University, 183 p. http://hdl.handle.net/10092/6783

Field, B.D., Browne, G.H., Davy, B.W., Herzer, R.H., Hoskins, R.H., Raine, J.I., Wilson, G.J., Sewell, R.J., Smale, D., Watters, W.A., 1989 Cretaceous and Cenozoic sedimentary basins and geological evolution of the Canterbury region, South Island, New Zealand. Lower Hutt: New Zealand Geological Survey. New Zealand Geological Survey basin studies 2. 94 p.

Finn, C. A., R. D. Müller., K. S. Panter., 2005, A Cenozoic diffuse alkaline magmatic province (DAMP) in the southwest Pacific without rift or plume origin: Geochemistry, Geophysics, Geosystems, https://doi.org/10.1029/2004GC000723

Fornaciai, A., M. Favalli., D. Karátson., S. Tarquini., E. Boschi., 2012, Morphometry of scoria cones, and their relation to geodynamic setting: A DEM-based analysis: Journal of Volcanology and Geothermal Research, doi:10.1016/j.jvolgeores.2011.12.012.

Forsyth, P.J., Barrell, D.J.A., Jongens, R., 2008, Geology of the Christchurch area. Institute of Geological and Nuclear Sciences 1:250,000 Geological Map 16. Lower Hutt, GNS Science. 67 p1 sheet.

Giba, M., J. J. Walsh, Andrew Nicol, V. Mouslopoulou, H. Seebeck., 2013, Investigation of the Spatio-Temporal Relationship between Normal Faulting and Arc Volcanism on Million-Year Time Scales. Journal of the Geological Society 170 (6): 951–62. https://doi.org/10.1144/jgs2012-121

Graettinger, A.H., G.A. Valentine, I., Sonder., 2016, Recycling in Debris-Filled Volcanic Vents. Geology 44, no. 10 (2016): 811. https://doi.org/10.1130/G38081.1

Hawkes, P. W., D. D. Mound., 1984, BP Shell Todd (Canterbury) Services Limited, Clipper-1 Geological Completion Report PR1036.

Holford, S. P., N. Schofield, J. D. MacDonald, I. R. Duddy, P. F. Green., 2012, Seismic Analysis of Igneous Systems in Sedimentary Basins and Their Impacts on Hydrocarbon Prospectivity: Examples from the Southern Australian Margin. APPEA Journal, 52, 229–52.

Hunt, D., and M. E. Tucker., 1992, Stranded parasequences and the forced regressive wedge systems tract: deposition during base-level fall: Sedimentary Geology, v. 81, no. 1–2, p. 1–9, https://doi.org/10.1016/0037-0738(92)90052-S

Huafeng, T. , Phiri, C. , Youfeng, G. , Yulong, H. and Weihua, B., 2015, Types and Characteristics of Volcanostratigraphic Boundaries and Their Oil-Gas Reservoir Significance. Acta Geologica Sinica - English Edition, 89: 163-174. https://doi.org/10.1111/1755-6724.12402

Iacono-Marziano, G., Morizet, Y., Le Trong, E., Gaillard, F., 2013, New experimental data and semi-empirical parameterization of H2O-CO2 solubility in mafic melts. Geochimica Et Cosmochimica Acta 97. 145-157.

Infante-Paez, L., and K. J. Marfurt, 2017, Seismic expression and geomorphology of igneous bodies: A Taranaki Basin, New Zealand, case study: Interpretation, v. 5, no. 3, p. SK121-SK140, https://doi.org/10.1190/INT-2016-0244.1

Jerram, D. A., R. T. Single., R. W. Hobbs., C. E. Nelson., 2009, Understanding the offshore flood basalt sequence using onshore volcanic facies analogues: An example from the Faroe-Shetland basin: Geological Magazine, https://doi.org/10.1017/S0016756809005974

Kamp, P. J. J., P. F. Green., J. M. Tippett., 1992, Tectonic architecture of the mountain front-foreland basin transition, South Island, New Zealand, assessed by fission track analysis: Tectonics, https://doi.org/10.1029/91TC02362

Kereszturi, G., K. Németh., 2013, Monogenetic Basaltic Volcanoes: Genetic Classification, Growth, Geomorphology and Degradation: Updates in Volcanology - New Advances in Understanding Volcanic Systems, https://doi.org/10.5772/51387

Lever, H., 2007, Review of unconformities in the late Eocene to early Miocene successions of the South Island, New Zealand: Ages, correlations, and causes: New Zealand Journal of Geology and Geophysics, v. 50, no. 3, p. 245-261.

Lu, H., C. S. Fulthorpe., P. Mann., M. A. Kominz., 2005, Miocene-Recent tectonic and climatic controls on sediment supply and sequence stratigraphy: Canterbury

basin, New Zealand: Basin Research, v. 17, no. 2, p. 311–328, https://doi.org/10.5772/5138710.1111/j.1365-2117.2005.00266.x

Marfurt, K., 2018, Seismic Attributes as the Framework for Data Integration Throughout the Oilfield Life Cycle: Society of Exploration Geophysicists, 508 p., https://doi.org/10.1190/1.9781560803522

McLean, C. E., N. Schofield., D. J. Brown., D. W. Jolley., and A. Reid, 2017, 3D seismic imaging of the shallow plumbing system beneath the Ben Nevis Monogenetic Volcanic Field: Faroe–Shetland Basin: Journal of the Geological Society, https://doi.org/10.1144/jgs2016-118

McPhie, J., M. Doyle., R. Allen., 1993, Volcanic textures - a guide to the interpretation of textures in volcanic rocks. Centre for Ore Deposit and Exploration Studies, University of Tasmania.

Milne, A.D., 1975. Well completion report Resolution, for BP, Shell, Todd Canterbury Service Limited. New Zealand Geological Survey Open-file Petroleum Report No. 648.

Mortimer, N., 2004, New Zealand's Geological Foundations: Gondwana Research, v. 7, no. 1, p. 261-272.

Nelson, S. T., A. Montana., 1992, Sieve-textured plagioclase in volcanic rocks produced by rapid decompression: American Mineralogist.

Pearce, T.H., 1993, Analcime phenocrysts in igneous rocks: Primary or secondary? Discussion. Am. Mineral. 78, 225-229.

Peretyazhko, I. S., 2010, Genesis of mineralized cavities (Miaroles) in granitic pegmatites and granites: Petrology, https://doi.org/10.1134/S0869591110020062

Planke, S., E. Alvestad, O. Eldholm., 1999, Seismic Characteristics of Basaltic Extrusive and Intrusive Rocks. The Leading Edge 18 (3): 342. https://doi.org/10.1190/1.1438289

Planke, S., P. A. Symonds, E. Alvestad, J. Skogseid., 2000, Seismic Volcanostratigraphy of Large-Volume Basaltic Extrusive Complexes on Rifted Margins. Journal of Geophysical Research 105 (B8): 19335. https://doi.org/10.1029/1999JB900005

Planke, S., J. M. Millett., D. Maharjan., D. A. Jerram., M. M. Abdelmalak., A. Groth., J. Hoffmann., C. Berndt., and R. Myklebust., 2017, Igneous seismic geomorphology of buried lava fields and coastal escarpments on the Vøring volcanic rifted margin: Interpretation, https://doi.org/10.1190/INT-2016-0164.1

Reynolds, P., N. Schofield., R. J. Brown., S. P. Holford., 2016, The architecture of submarine monogenetic volcanoes - insights from 3D seismic data: Basin Research, v. 30, p. 437–451, https://doi.org/10.1111/bre.12230

Robertson, J., E. M. Ripley., S. J. Barnes., C. Li, 2015., Sulfur liberation from country rocks and incorporation in mafic magmas: Economic Geology, https://doi.org/10.2113/econgeo.110.4.1111

Schofield, N., D. A. Jerram., S. Holford., A. Stuart., M. Niall., A. Hartley., J. Howell., M. David., P. Green., D. Hutton., C. Stevenson., 2016, Sills in sedimentary basin and petroleum systems, in K. Németh, ed., The Series Advances in Volcanology, 1–22.

Sewell, R. J., 1988, Late Miocene volcanic stratigraphy of central Banks Peninsula, Canterbury, New Zealand: p. 41–64, https://doi.org/10.1080/00288306.1988.10417809

Silva, S. D., J. M. Lindsay., 2015, Primary Volcanic Landforms. The Encyclopedia of Volcanoes. https://doi.org/10.1016/B978-0-12-385938-9.00015-8

Single, R.T., Jerram, D.A., 2004. The 3-D facies architecture of flood basalt provinces and their internal heterogeneity: examples from the Palaeogene Skye Lava Field. Journal of the Geological Society 161, 911-926

Smith, K. L., A. R. Milnes., R. A. Eggleton., 1987, Weathering of basalt: formation of iddingsite. Clays Clay Miner. 35, 418– 428.

Schiøler, P., Raine, J.I., A. Griffin., C.J. Hollis., D.K. Kulhanek., H.E.G. Morgans., L. Roncaglia., C.P. Strong., C. Uruski., 2011. Revised biostratigraphy and well correlation, Canterbury Basin, New Zealand. GNS Science Consultancy Report 2011/12. 142 p.

Strogen, D. P., H. Seebeck., A. Nicol, P. R. King., 2017, Two-phase Cretaceous–Paleocene rifting in the Taranaki Basin region, New Zealand; implications for Gondwana break-up: Journal of the Geological Society, https://doi.org/10.1144/jgs2016-160

Stroncik, N. A., H. U. Schmincke., 2002, Palagonite - A review: International Journal of Earth Sciences, https://doi.org/10.1007/s00531-001-0238-7

Suggate, R.P., Stevens, G.R.,Te Punga, M.T., 1978, The geology of New Zealand. Govt Printer, Wellington.

Svensen, H. H., T. H. Torsvik., S. Callegaro., L. Augland., T. H. Heimdal., D. A. Jerram., S. Planke., and E. Pereira., 2017, Gondwana Large Igneous Provinces:

plate reconstructions, volcanic basins and sill volumes: Geological Society, London, Special Publications, https://doi.org/10.1144/SP463.7

Timm, C., K. Hoernle., R. Werner., F. Hauff., P. van den Bogaard., J. White., N. Mortimer., D. Garbe-Schönberg., 2010, Temporal and geochemical evolution of the Cenozoic intraplate volcanism of Zealandia: https://doi.org/10.1016/j.earscirev.2009.10.002

Walker, F., 1957, Ophitic Texture and Basaltic Crystallization. The Journal of Geology, 65(1), 1-14. Retrieved from http://www.jstor.org/stable/30064199.

Walker, G. P. L., R. Croasdale., 1971, Characteristics of some basaltic pyroclastics: Bulletin Volcanologique, https://doi.org/10.1007/BF02596957

White, J. D. L., 2000, Subaqueous eruption-fed density currents and their deposits: Precambrian Research, 101 (2000) 87–109 https://doi.org/10.1016/S0301-9268(99)00096-0

White, J. D. L., P. S. Ross., 2011, Maar-diatreme volcanoes: A review: https://doi.org/10.1016/j.jvolgeores.2011.01.010